MEASURING DEPROTECTION KINETICS IN CHEMICALLY AMPLIFIED RESISTS WITH IN-SITU INFRARED SPECTROSCOPY

A Thesis

Presented to

the Faculty of the Department of Chemical Engineering

University of Houston

In Partial Fulfillment

of the Requirements for the Degree

Master of Science

in Chemical Engineering

by

Minnie Lahoti

May 2016

MEASURING DEPROTECTION KINETICS IN CHEMICALLY AMPLIFIED RESISTS WITH IN-SITU INFRARED SPECTROSCOPY

Minnie Lahoti

Approved:

Chair of the Committee
Dr. Gila Stein, Associate Professor,
Chemical and Biomolecular Engineering

Committee Members:

Dr. Jack Wolfe, Professor,
Electrical Engineering

Dr. Michael P. Harold, M.D. Anderson Professor
Chemical and Biomolecular Engineering

Dr. Suresh K. Khator, Associate Dean,
Cullen College of Engineering

Dr. Michael P. Harold, M.D. Anderson
Professor, Chair
Chemical and Biomolecular Engineering

ACKNOWLEDGEMENTS

I would like to thank my Advisor, Dr. Gila Stein, for being the best mentor one could ask for. She took the time out of her busy schedule to answer all my questions and help me in all my endeavors. I would also like to thank Abhijit Patil, whose project I took over, for guiding me and teaching me how to use all the lab equipments. I also owe a big thanks to my committee members, Dr. Jack Wolfe and Dr. Michael Harold, for taking the time to review my thesis and serving on my committee. Finally, I would like to thank my parents, Mukta and Vikas Lahoti, and my Aunt and Uncle, Angela Summers and Sanjeev Lahoti; without their love and support I would not even be here in the first place.

MEASURING DEPROTECTION KINETICS IN CHEMICALLY AMPLIFIED RESISTS WITH IN-SITU INFRARED SPECTROSCOPY

An Abstract

Of a

Thesis

Presented to

the Faculty of the Department of Chemical Engineering

University of Houston

In Partial Fulfillment

of the Requirements for the Degree

Master of Science

in Chemical Engineering

by

Minnie Lahoti

May 2016

ABSTRACT

Chemically amplified photoresists have been used in semiconductor lithography for over 40 years. These materials are based on an acid-sensitive polymer containing a low concentration of a strong acid catalyst. Patterns are formed in the polymer through a coupled reaction-diffusion process. The diffusion length of the acid catalyst may control the pattern dimensions, which is a significant challenge for future manufacturing processes that need to resolve features at the scale of 10 nm. The goal of this project is to develop predictive models of pattern formation using a model photoresist system. First, reaction kinetics was measured with in-situ infrared absorbance spectroscopy as a function of temperature (below the glass transition temperature), acid catalyst concentration, and acid-anion size. These data demonstrate that a smaller acid-anion pair leads to faster reactions. Second, conversion kinetics was analyzed with a simple model of reaction with slow catalyst loss. The model qualitatively captures the observed trends and suggests an activation energy on the order of 100 kJ/mol for each catalyst/polymer system, which is the magnitude expected for a diffusion-controlled reaction in a glassy polymer. Collectively, these outcomes demonstrate that pattern formation in chemically amplified photoresists is largely controlled by acid catalyst diffusion.

Table of Contents

ACKNOWLEDGEMENTS v
ABSTRACT vii

Table of Contents viii

List of Figures x

List of Tables xii

CHAPTER 1: INTRODUCTION 1

Photolithography 1
Chemically Amplified Photoresists 2
Environmentally Stable Chemically Amplified Positive (ESCAP) resist 4
CHAPTER 2: REACTION AND DIFFUSION IN POLYMERS 6

Diffusion in Liquids and Solids 6
Diffusion in Polymers 8
Reaction Diffusion Experiments 11
Single Layer Experiments 13
Bilayer Experiments 15
Trilayer Experiments 19
Acid catalyzed deprotection kinetics model 22
CHAPTER 3: INFRARED SPECTROSCOPY 25

Materials 25
Reactions 25
Sample Preparation 33
Using FTIR 34
CHAPTER 4: RESULTS AND DISCUSSION 37

Inactive Catalyst 37
Kinetics at low temperature 38

Initial Deprotection Level Calculations 39
Modeling Deprotection Rates 41
CHAPTER 5: FUTURE WORK 48
BIBLIOGRAPHY 53

List of Figures

Figure 1. Schematic diagram of Photolithography. 2

Figure 2. a) A solution of polymer (black and red dots) with catalyst (blue) in PGMEA (light blue) is spincoated on a silicon wafer (black). The red dots on the polymer are acid sensitive group. The acid in the photoresist is activated using UV light. b) shows the activated catalyst in the polymer matrix, ready to react with the acid sensitive groups on the polymer. c) shows the positive tone resist pattern formed when treated with developer solution to wash away the deprotected polymer. 4

Figure 3. Skin and T-top formation in photoresist..... 4

Figure 4. Schematic of hole hopping diffusion mechanism. 7

Figure 5. Interstitial diffusion of solutes through a lattice..... 7

Figure 6. Grain boundary diffusion. 8

Figure 7. Free volume theory depiction in polymers as it transitions from glassy to melt. 10

Figure 8. Schematic of a bilayer experiment technique..... 12

Figure 9. Trilayer consisting of acid feeder, polymer, and acid detector layers..... 13

Figure 10. Acid diffusion through polymer matrix via secondary interactions..... 14

Figure 11. Step by step process to produce a bilayer of Novolac and PTSA. 16

Figure 12. Schematic for Bilayer experiment done by Lin et al..... 18

Figure 13. Polymer film stack used to measure diffusion rates..... 21

Figure 14. Reaction scheme for a) small acid generation b) bulky acid generation c) Deprotection reaction between polymer and photoacid..... 26

Figure 15. IR spectrum of poly(tert-butyl acrylate) (PtBA) 28

Figure 16. IR spectrum of poly(4-hydroxystyrene) (PHOST) 29

Figure 17. IR spectrum of Polystyrene (PS) 30

Figure 18. IR spectrum of polyacrylic acid (PAA) 31

Figure 19. IR spectrum of terpolymer with labeled characteristic peaks from each monomer moiety 32

Figure 20. Flowchart showing how raw data from the FTIR is converted to Deprotection level vs. time curve 35

Figure 21. Comparison of active and inactive catalyst when heated from 25 °C to 85 °C. 37

Figure 22. Deprotection level for 14.5×10^{-2} nm^{-3} active triflate vs. temperature and time. 38

Figure 23. Deprotection Level vs. time for PFBS and triflate at 40 °C. 39

Figure 24. K_p and K_t plots for triflate. Solid lines are predicted profiles basd on best-fit results for an acid concentration of 6.42×10^{-2} nm^{-3}. 42

Figure 25. K_p and K_t plots for PFBS. 43

Figure 26. Arrhenius plots for Triflate and PFBS 44

Figure 27. 2 cycles of Tg measurements for polymer with 14.5×10^{-2} nm^{-3} triflate. 46

Figure 28. PS film spin-coated on top of a pure polymer film and heated at 110 °C. 50

Figure 29. PS film spin-coated on top of a polymer and inactive catalyst and heated. 50

Figure 30. PS film spin-coated on top of a deprotected polymer film and then heated.... 51

Figure 31. PS film spin-coated on top of a polymer film with active catalyst. The film was deprotected and dewetted at 110 °C. 51

List of Tables

Table 1. Diffusion coefficients of penetration through solids, liquid, gases, and polymers. 11

Table 2. Diffusion coefficients near glass transition temperature. 21

Table 3. IR peak assignments for 4 homopolymers[33,37] 33

Table 4. Summary of reactions that were reproducible or not for Triflate. 36

Table 5. Summary of reactions that were reproducible or not for PFBS. 36

Table 6. Instantaneous deprotection level for each acid concentration. 41

Table 7. Parameters extracted from Arrhenius plots. 44

Table 8. T_g measurements taken for polymer with different triflate concentrations. 46

Table 9. T_g measurements taken for polymer with different triflate concentrations. 46

Table 10. Dewetting experiments with PS and triflate. 49

Table 11. Thickness measurement before and after immersion in toluene for 20 seconds. 52

CHAPTER 1: INTRODUCTION

The integrated circuits industry has seen enormous growth over the past 50 years. In 1965 the co-founder of Intel, Gordon Moore, predicted that the number of transistors per central processing unit (CPU) would double almost every two years[1]. Remarkably, the industry did maintain this growth for several decades. However, since Intel came out with the 22 nm node manufacturing process in 2012, the growth rate has dwindled. One factor that limits this growth is being able to manufacture transistors at the nanometer scale. Hence, there is an imperative need to overcome this barrier to keep up with the demand to produce low cost integrated circuits and other semiconductor devices. Several steps are required to produce an integrated circuit, but it is the lithographic step that limits the minimum printable feature size.

Photolithography

Lithography is a printing technique that was discovered by Alois Senefelder in 1798 to publish his theatrical works[2]. In the 1950s, lithography evolved from an artistic printmaking medium, which originally used "stamps" made from gum arabic and limestone, to a fabrication technique for intricate patterns on integrated circuits. Lithography in the semiconductor industry uses ultraviolet light to pattern a radiation-sensitive coating on a silicon wafer. This technique is known as photolithography or projection lithography[2].

Figure 1 illustrates the basic steps in a typical photolithography process. A silicon wafer is coated with a radiation sensitive polymer film and then exposed to light through a patterned mask. Exposure to light initiates a chemical reaction that changes the

solubility of the polymer film. Depending on the chemistry, either the exposed film washes away with the developer (positive tone) or the unexposed region washes away (negative tone).

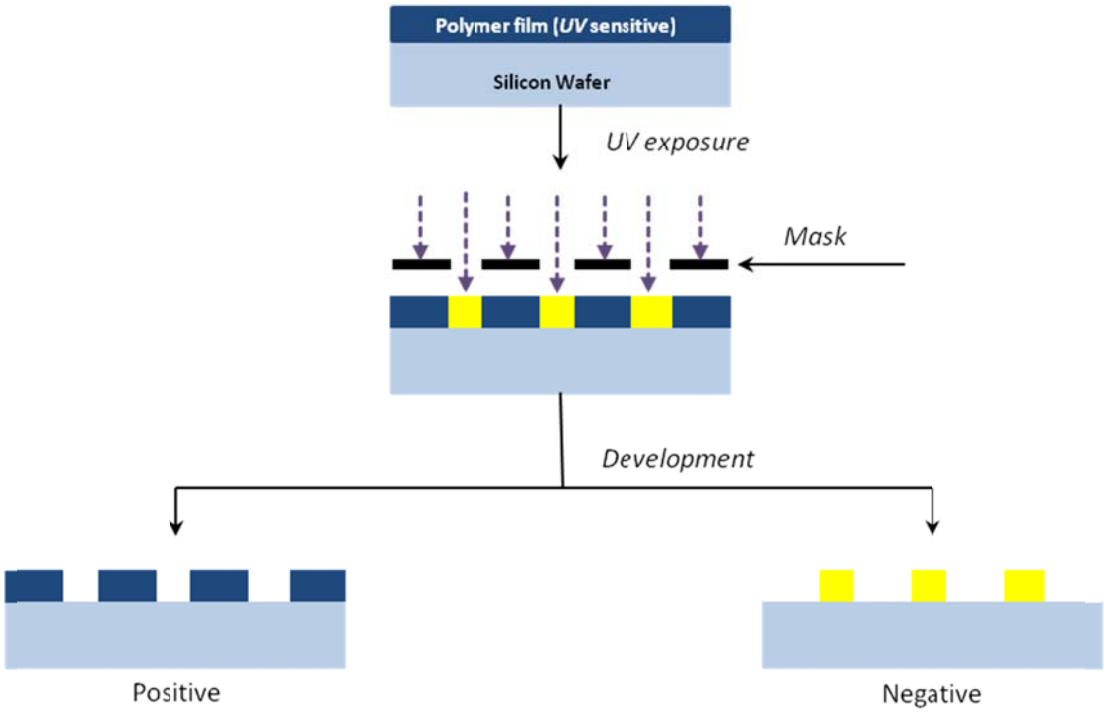

Figure 1. Schematic diagram of Photolithography.

Chemically Amplified Photoresists

IBM researchers introduced the concept of chemical amplification in 1980. The resist systems used before then had limited sensitivity to radiation because they were based on a photochemical reaction that required several photons to generate one product[3]. The past several decades has seen tremendous growth in the use of chemically amplified photoresists in industrial lithography due to their high sensitivity to radiation and excellent patterning abilities. A film comprised of a polymer with acid-sensitive groups and a photoacid generator makes up a photoresist. Photoacid generators are compounds

that generate acids upon irradiation with light. There are two types of photoacid generators, namely, ionic and non-ionic. Ionic compounds are preferred because of their higher thermal stability, as compared to non-ionic compounds[4].

Figure 2 illustrates the solubility-switching reaction in photolithography with chemically amplified resists. The polymer and catalyst are dissolved in a solvent and then spincoated on a silicon wafer. The film is heated to drive off volatile contaminants and excess solvent, a step commonly referred to as the post-apply bake (PAB). Next, ultraviolet (UV) light activates a pattern of photoacid generators as shown in Figure 2a. The film is then heated so the acid can diffuse through the polymer and catalyze deprotection reactions with the acid-sensitive groups in the polymer; this step is known as the Post Exposure Bake (PEB), and is illustrated in Figure 2b. Each reaction involves an acid deprotecting the polymer and regenerating the acid, so the photochemistry is "amplified" through the series acid-catalyzed reactions[3,5]. Thermal deprotection can also occur if the temperature is high enough to overcome the activation energy barrier for deprotection, but the PEB temperature is selected to be below this threshold. The deprotection chemistry is designed to change the polymer's polarity and solubility so exposed (or un-exposed) regions are selectively dissolved to produce nanoporous template of Figure 2c.

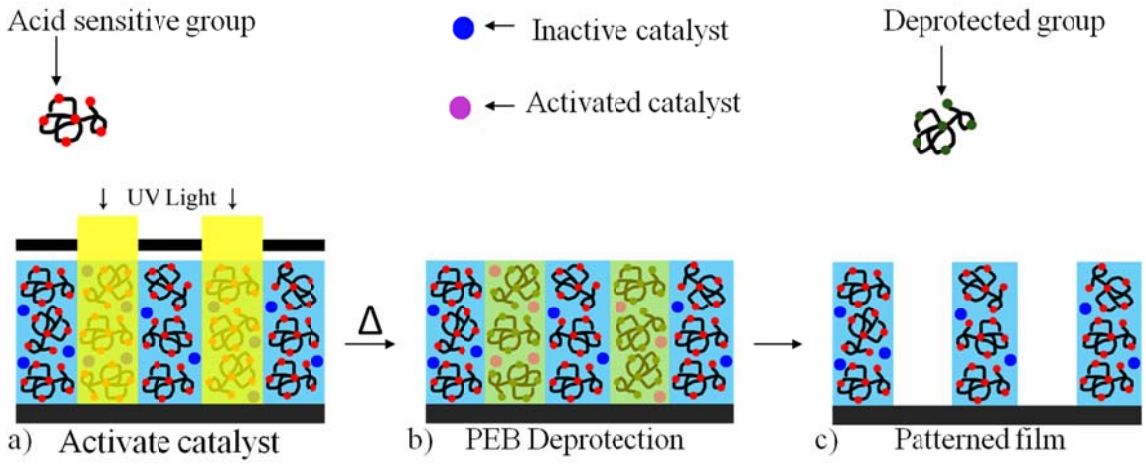

Figure 2. a) Activation of catalyst using UV light. b) shows the activated catalyst ready to react with the acid sensitive groups on the polymer. c) shows the positive tone resist pattern formed.

Environmentally Stable Chemically Amplified Positive (ESCAP) resist

In 1980s, IBM researchers observed a delay in the chemical amplification due to the presence of airborne N-methylpyrrolidone (NMP) at ppb levels during the PEB step. The "T-topping" effect (shown in Figure 3) was observed when NMP adsorbed on the resist surface and neutralized the acid catalyst. As a result, this would cause a delay in the chemical amplification process.

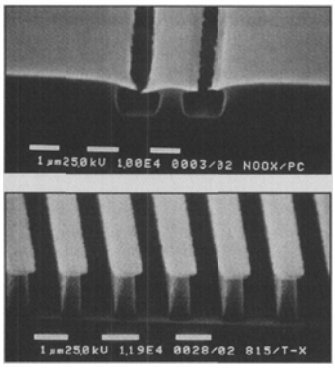

Figure 3. Skin and T-top formation in photoresist[3].

They proposed two ways to overcome the NMP contamination problem. First, lowering the activation energy of deprotection would cause deprotection to occur at room temperature thereby skipping the PEB step in which the contamination occurs. However, most resists require the PEB step for the acid-catalyzed reaction to occur so this was not a viable option. Next they proposed that the chances of NMP adsorbing could be diminished by reducing the free volume in the polymer film. One way to reduce the free volume is to use a polymer film with a glass transition temperature that is below the threshold for thermal deprotection. When the film is heated near its glass transition temperature, the polymer film densifies as solvent is removed, thereby reducing the free volume. Smaller free volume means less NMP is adsorbed on the film. Based on this annealing concept, a new resist, known as Environmentally Stable Chemically Amplified Positive (ESCAP) resist, was designed to overcome NMP contamination problem[3].

The ESCAP resists are usually comprised of hydroxystyrene and t-butyl acrylate monomers in a random sequence, sometimes with other co-monomers like styrene. It can be baked at temperatures as high as 150 °C without premature thermal deprotection, so residual solvent can be driven out of the film prior to acid activation. Therefore, it offers excellent thermal stability and overcomes the chemical amplification delay problem[3]. As these systems are easy to use (not sensitive to contamination), they are popular model systems for academic research. Fundamental studies of acid-catalyzed deprotection kinetics and acid diffusion in ESCAP formulas are reviewed in Chapter 2.

CHAPTER 2: REACTION AND DIFFUSION IN POLYMERS

Diffusion in Liquids and Solids

Diffusion in liquids is easy to understand and observed in our everyday lives. The motion and interaction of molecules in liquids is chaotic. Even though liquid molecules are held together through weak or strong secondary interactions, they are forgiving enough that the motion of the particles is easily achieved. Unlike liquids, diffusion in solids is extremely slow due to the close packed configuration of atoms. The most common types of solids have polycrystalline structure in which the main pathway of diffusion is through lattice defects. There are three ways by which solute molecules can diffuse through a solid: hole hopping (Figure 4), interstitial diffusion (Figure 5), and grain boundary diffusion (Figure 6). Diffusion in amorphous solids occurs through similar but non-uniform mechanisms. When a solute molecule moves from one lattice site to an empty lattice site (vacancy defect) and so forth, it is known as hole hopping diffusion. If the solute particle diffusing through is small, then it can traverse via the intramolecular voids or interstices, hence the name interstitial diffusion. A defect in crystal lattice can allow a solute molecule to move in between lattice defects as shown in Figure 6. Diffusion through such a defect is called grain boundary diffusion.

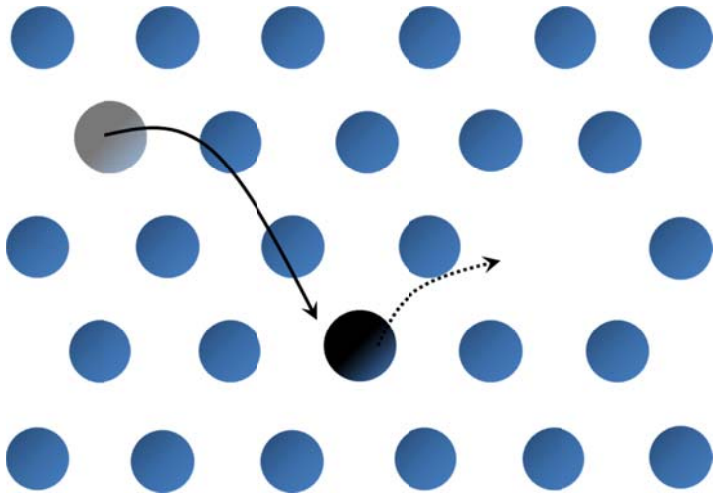

Figure 4. Schematic of hole hopping diffusion mechanism.

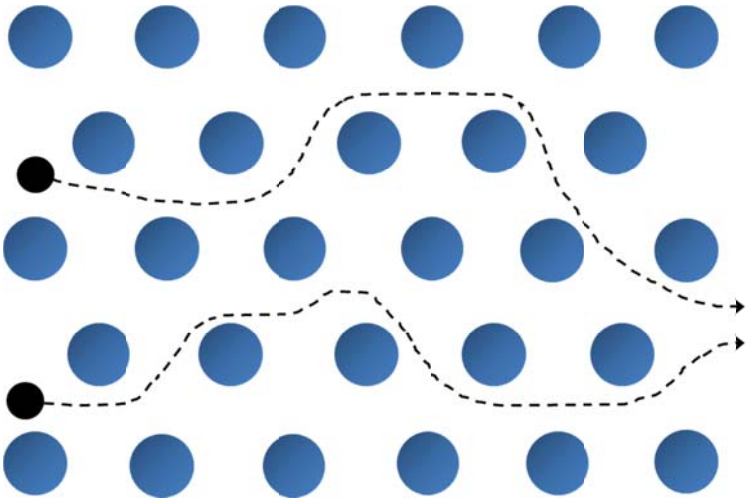

Figure 5. Interstitial diffusion of solutes through a lattice.

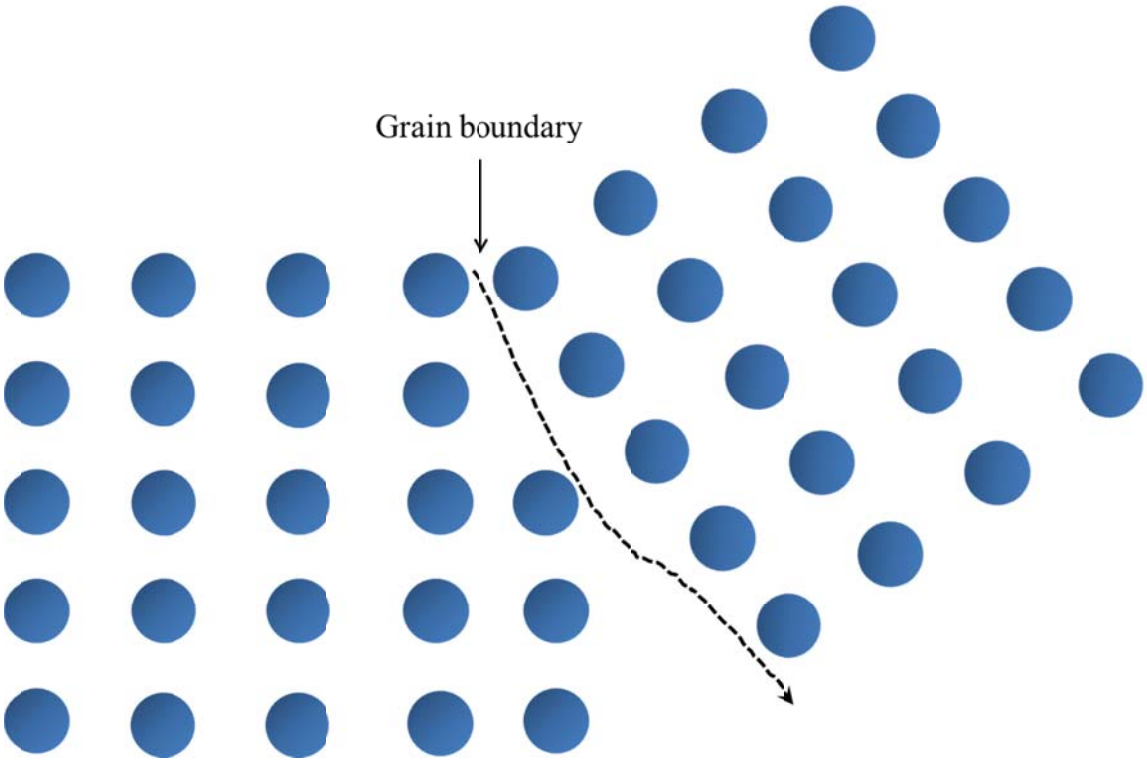

Figure 6. Grain boundary diffusion.

Diffusion in Polymers

Diffusion in polymers is harder to understand since they have characteristics that are both solid-like and liquid-like. Most polymers show a transition from a glassy state to melt state over a range of temperatures. The midpoint of this temperature is known as the glass transition temperature (T_g). The transition is accompanied by the freeing of hindered rotations of —C—C— bonds in the polymer chain[6]. A polymer above its T_g acts like a high viscosity liquid; below the T_g a polymer is glassy, resembling a low density solid. When a polymer is in its melt state, it is flexible and mobile, and solutes can easily traverse through the matrix.

The rate of diffusion of a molecule through a polymer matrix changes with size of the molecule and the temperature at which diffusion occurs. The glass transition

temperature (T_g) also plays an important role in determining diffusivity. Diffusivity is highly dependent on the sample temperature relative to the polymer's T_g [7–9]. The volumes of the photoacids are large enough that the diffusion is controlled by the chain dynamics of the polymer matrix. Diffusion below T_g is described by the Arrhenius equation and can be thought of as a thermally activated process. Above the T_g, the temperature dependence can be calculated using the Williams-Landel-Ferry (WLF) equation. The WLF relates the temperature dependence of chain relaxation time to free volume. The free volume fraction is roughly the same in all polymers at glass transition temperature so if the diffusion coefficient of the photoacid is known in a polymer at its Tg[10], it is possible to estimate the diffusivity of the same photoacid in a different polymer matrix using WLF[11,12].

Polymers in their glassy state have limited mobility as the polymer chains are densely packed and have no large-scale freedom of rotation. However, there are "holes" present in the polymer matrix that can be used by the solute particles to travel through. These holes are either fixed in place or change position with time[13]. The free volume theory best describes diffusion through glassy polymer. The foundation of the free volume theory is based on three different types of specific volumes occupied by the polymer and the penetrant molecule, illustrated in Figure 7.

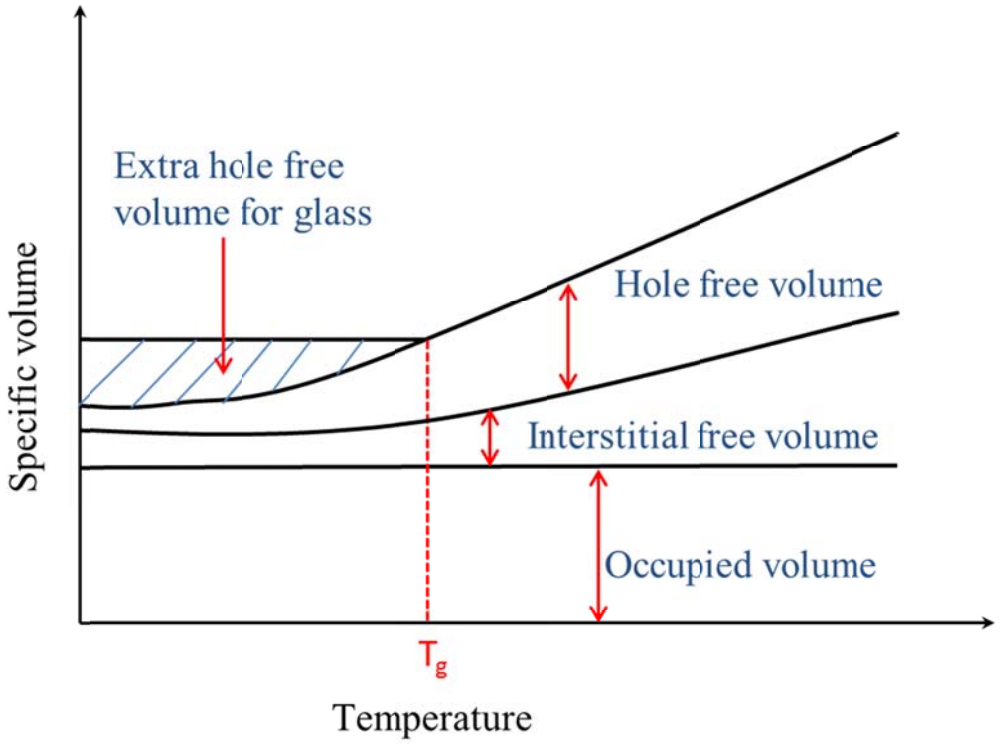

Figure 7. Free volume theory depiction in polymers as it transitions from glassy to melt.

The fixed volume occupied by the molecules is known as the specific occupied volume. The rest of the volume is called the free volume. There are two type of free volumes, namely, interstitial and hole free volume. Interstitial free volume is uniformly distributed within the polymer matrix and requires a large amount of energy for redistribution and therefore, is not affected by thermal fluctuations. Hole free volume is constantly being redistributed due to random thermal fluctuations. The extra hole free volume for glassy state can be reduced by annealing the polymer and in turn changing its properties. According to the free volume theory of diffusion, the penetrant movement is determined by the amount of free hole volume and the size of the penetrant molecule[14].

Table 1 compares diffusion coefficients for solids, liquids, gases, and polymers; it is observed that solids have the smallest diffusion coefficients. Polymers below their T_g act like pseudo-solids. Polymers above T_g are more liquid-like in nature and have slightly higher diffusion coefficients as compared to polymers below T_g.

Table 1. Diffusion coefficients of penetration through solids, liquid, gases, and polymers.

	D (cm^2/s)	**Conditions**
Gases[11]	0.09 – 0.2	1 atm, 25 °C
Liquids [11]	0.8×10^{-5} Ethanol in water	At infinite dilution in water at 25 °C
	1.2×10^{-5} Acetic acid in water	
	1×10^{-5} Benzene in water	
Solids[11]	3×10^{-48} Fe through Fe (BCC)	At 25 °C
	6×10^{-21} C through Fe (BCC)	
	2×10^{-38} Zn through Cu	
Polymers[12] **(above T_g)**	$10^{-11} – 10^{-9}$	Protected polymer with active PAG
Polymers[13] **(below T_g)**	$5x10^{-16} – 1.5\times10^{-13}$ (Deprotected Polymer)	For various PAG, polymers, PEB temperatures
	$4x10^{-17} – 1\times10^{-15}$ (Protected Polymer)	

Reaction Diffusion Experiments

As mentioned earlier, it is the lithographic step that limits the feature sizes that can be achieved in photoresists. Image blur due to diffusion has been studied for several decades now. Acid diffusion depends on the residual solvent in the photoresist[15], glass transition temperature of the polymer, the molecular size of the acid generators[16], baking temperature, and extent of reaction[17,18]. Most photoresists are processed at temperatures

below T_g. The acid-catalyzed reaction changes the polarity of the polymer matrix. The deprotected polymer has polar sites that can trap the acid and cause diffusion to slow down. Several types of experiments have been conducted in order to extract diffusion rates. However, all the experiments can be categorized into three types:

Single Layer. A solution of polymer and catalyst is spincoated on a silicon wafer. There is no macroscale concentration gradient of acid-catalyst in any direction. The experiment measures the rate of deprotection by monitoring the concentration of protecting groups as a function of time. Diffusion coefficients cannot be directly measured but have to be extracted from a kinetics model that fits the experimental data. Figure 2 shows an example of a single layer.

Bilayer. In this type of film the catalyst is present in a layer above the polymer layer. The catalyst then diffuses into the polymer layer, as shown in Figure 8. After some time of heating, a new boundary layer forms where the deprotection has occurred (shown in green). The Experiment measures the width of the boundary layer to extract the diffusion length, or monitors a signal in the polymer layer that is associated with acid arrival.

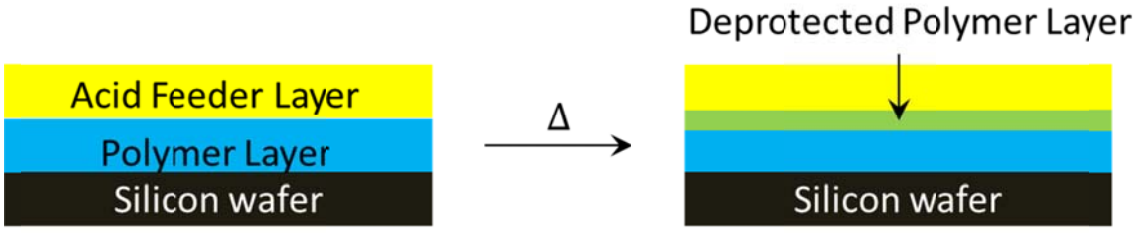

Figure 8. Schematic of a bilayer experiment technique.

Trilayer. A polymer film is sandwiched between an acid feeder layer and an acid detector layer. The acid diffuses from the feeder layer through the polymer film, and the

detector emits a signal when the acid arrives. The diffusion time (arrival time) through a known thickness of the polymer film is used to calculate the diffusion coefficient. A typical trilayer approach is depicted in Figure 9.

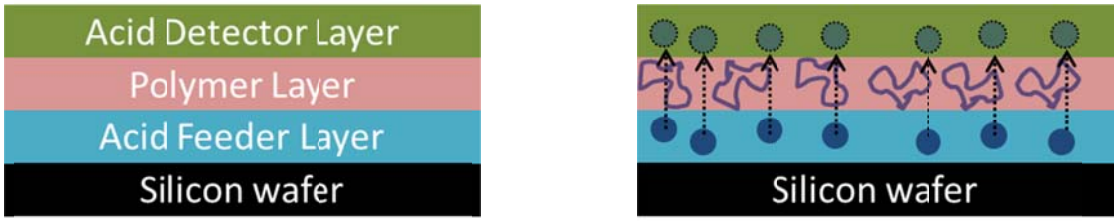

Figure 9. Trilayer consisting of acid feeder, polymer, and acid detector layers.

Single Layer Experiments

The most basic experiments carried out by researchers include a single layer of polymer and acid catalyst spincoated on a substrate. Diffusion lengths cannot be directly measured in these experiments, but diffusion coefficients can be calculated from indirect measurements with an appropriate model.

Itani et al. used conductivity measurements to explore acid diffusion behavior of tert-butoxycarbonyl (t-BOC) (T_g ~125 °C[19]) protected chemically amplified resist, with 2,4-dimethylbenzenesulfonic acid (DBS) as the PAG, for various prebake temperatures below T_g of t-BOC. The prebake temperature controls the amount of solvent in the resist. They confirmed that the residual solvent is directly related to the acid diffusion length. The diffusion coefficient *D* and diffusion length *L* were obtained using Fick's Law,

$$D = \sigma k_B T/[H]q^2 \text{ and} \quad (1)$$

$$L = (2Dt)^{\frac{1}{2}}, \quad (2)$$

where, σ, k_B ,T, [H], q, and t are ion conductivity, Boltzmann constant, diffusion temperature, amount of acid, ionic charge, and diffusion time, respectively. [H] and q were measured values. *D* values ranged from 3×10^{-14} cm^2/s to 2×10^{-13} cm^2/s while the diffusion lengths ranged from 10 nm to 50 nm, for prebake temperature range of 90 °C – 150 °C. The following figure shows the proposed mechanism for acid [H] diffusion via hydrophilic –OH sites in the residual solvent.

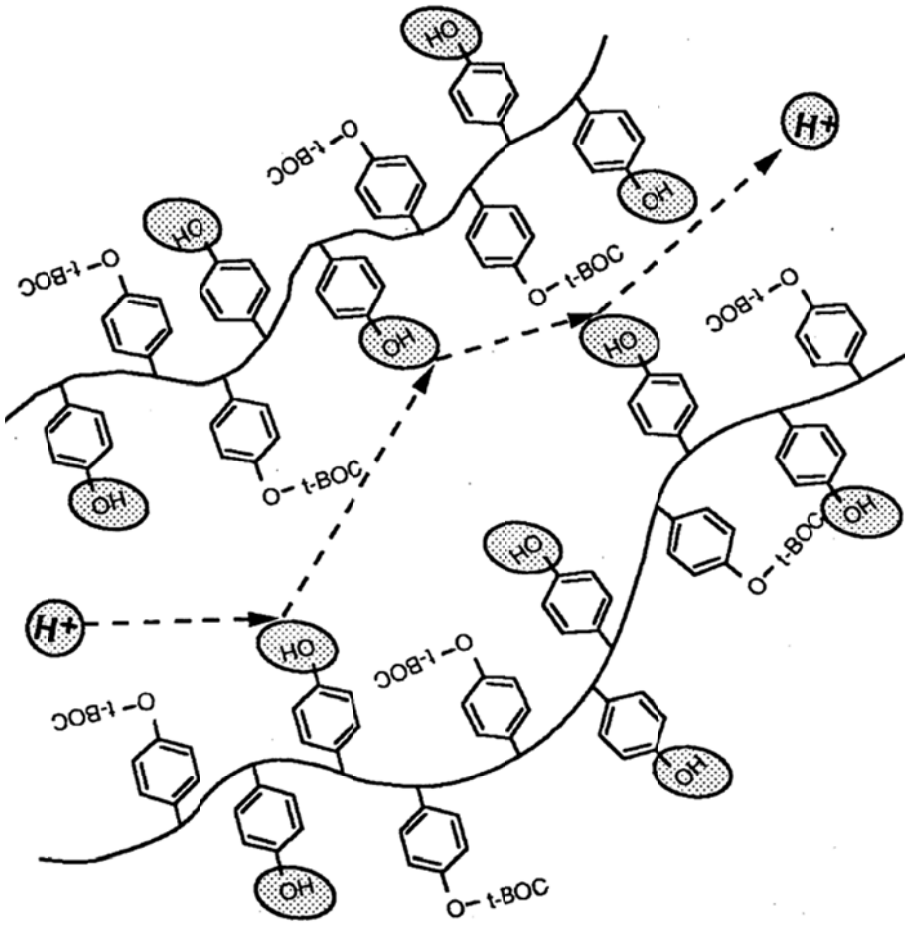

Figure 10. Acid diffusion through polymer matrix via secondary interactions[20].

Thus, the relationship between residual solvent and diffusion length was confirmed. A faster diffusion was observed when a higher amount of residual solvent was

present. Also, two diffusion pathways of the acid catalyst were confirmed with the help of the residual solvent and the –OH site of the polymer matrix.

Perera et al. used a glassy poly(4-hydroxystyerene-co-tert-butylacrylate) (PHOST-PTBA) with triphenylsulfonium perfluro-1-butanesulfonate (PFBS) as a photoacid generator to measure acid catalyzed deprotection rates using infrared spectroscopy and stochastic simulations to model the reaction-diffusion processes. These studies assumed that deprotection in glassy films is a diffusion-controlled process. The diffusion coefficient in the deprotected state was estimated from a non-Fickian model of acid transport, and ranged 10^{-15} to 10^{-14} cm^2/s at temperatures well below the glass transition.

Bilayer Experiments

Fryer et al. used bilayer samples of a film consisting of Novolac and *p*-toluene sulfonic acid (PTSA) to calculate diffusion coefficients at different catalyst concentration and temperatures. The T_g of Novolac was measured around 91 °C and the diffusion coefficients were measured below and above T_g. A schematic of the different steps involved in producing a bilayer is shown in Figure 11. A ~220 nm film of Novolac is spincoated on a silicon wafer (black). On another silicon wafer, maltose sugar is cast using DI water. Next, a layer of Novolac/PTSA is spincoated on top of the sugar film. This bilayer is placed in water where the sugar dissolves leaving the Novolac/PTSA layer to float on top of the water. This layer is then transferred on top of the pure Novolac to get the final bilayer.

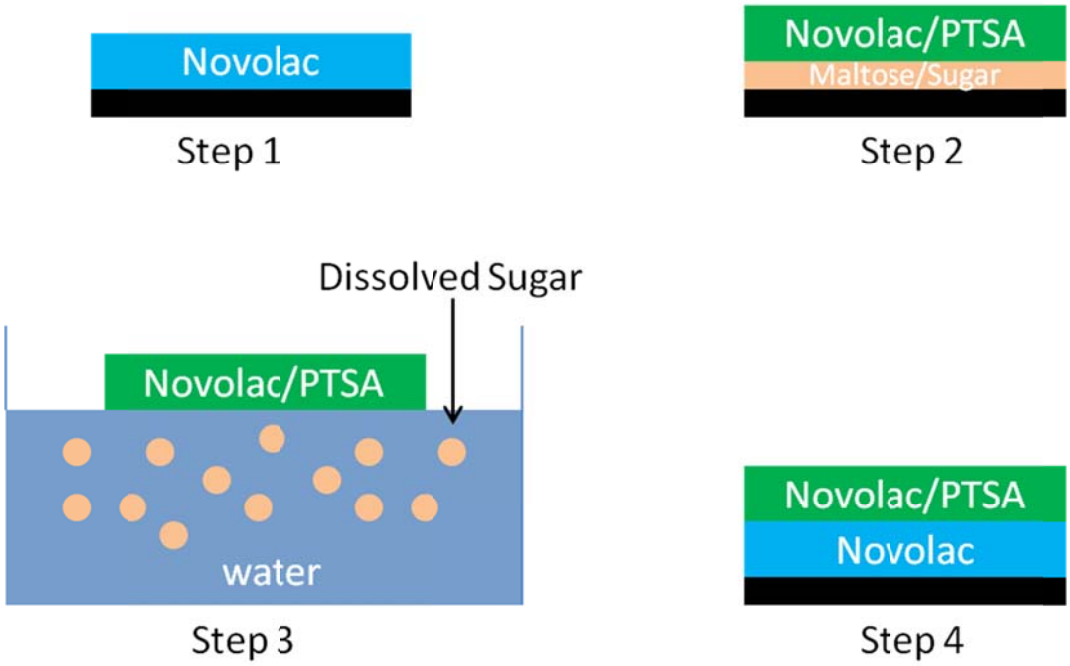

Figure 11. Step by step process to produce a bilayer of Novolac and PTSA.

The diffusion coefficient was obtained using a Fickian model of diffusion and the experimentally determined dependence of the refractive index (using an ellipsometer) as a function of the acid concentration. They assumed that the acid flux would follow Fick's law with a constant diffusion coefficient. Diffusion lengths varied from 11 nm to 141 nm when temperature ranged from 50 °C to 95 °C, corresponding with diffusion in the range of 10^{-15} to 10^{-12} cm^2/s for the same temperatures[12].

Goldfarb et al. explored a bilayer system consisting of protected polymer p-*tert*-butoxycarboxystyrene (PBOCST) as the bottom layer and a deprotected polymer poly(4-hydroxystyrene (PHOST) loaded with a photoacid generator Di-(*t*-butylphenyl) iodonium perfluorooctanesulfonate (PFOS) as the bottom layer. The main difference between Goldfarb's and Fryer's resist system was that Fryer used the protected polymer in both top and bottom layer. Goldfarb analyzed the spatial extent of the reaction front, or line edge,

between the deprotected and protected regions in the resist material by measuring the residual film thickness after immersing the stack in a good solvent for the protected film. The deprotected polymer is below its T_g during PEB while the protected polymer was examined both above and below its T_g. The glassy deprotected polymer only allows a certain amount of acid to diffuse into the protected polymer as a function of bake time. Whereas, for the case of the protected polymer in melt state, the velocity of the reaction front into the protected polymer is faster and is independent of the bake temperature. For a glassy protected polymer, the diffusion is slower and approximated using a Fickian diffusion model (similar to Fryer et al.). The diffusion coefficients for the melt and glassy protected polymer are of the order 10^{-14} - 10^{-12} cm^2/s and 10^{-16} - 10^{-13} cm^2/s, respectively[21].

Fryer and Goldfarb did not use a direct method to measure the reaction front in chemically amplified resist. However, Lin et al. explored the use of x-ray and neutron reflectometry to directly measure the spatial evolution of the reaction-diffusion process with nanoscale resolution. They used a resist system similar to Goldfarb's, but hydrogen was replaced with deuterium in the protected group of the polymer. Deuterium provides a strong contrast in neutron reflectivity without changing the chemistry of the system. A schematic of the bilayer resist system is shown in Figure 12. PBOCST (protected polymer) is spin-coated on a silicon substrate in step 1. A solution of PHOST (deprotected polymer) with PFOS is spin-coated on top of the PBOCST film (step 2). The catalyst is activated to produce acid (step 3). During PEB, the film thickness changes as the deprotection reaction proceeds (step 4). The top film is removed by developing the

resist in tetramethylammonium hydroxide (TMAH) solution (step 5). This top film is the sample they measure.

Thicknesses in step 1 and step 2 (PHOST layer) are 53.4 nm and 71.1 nm, respectively. The deprotected polymer film is 4 -20 nm thick. The observed deprotection polymer film is a result of the propagation of acid-catalyzed reaction and not thermal deprotection. Lin et al. also confirmed the non-Fickian shape by neutron and x-ray reflectivity. They were able to measure the density and composition profiles of the deprotecting polymer film. They substituted hydrogens with deuterium in order to use neutron reflectivity[22].

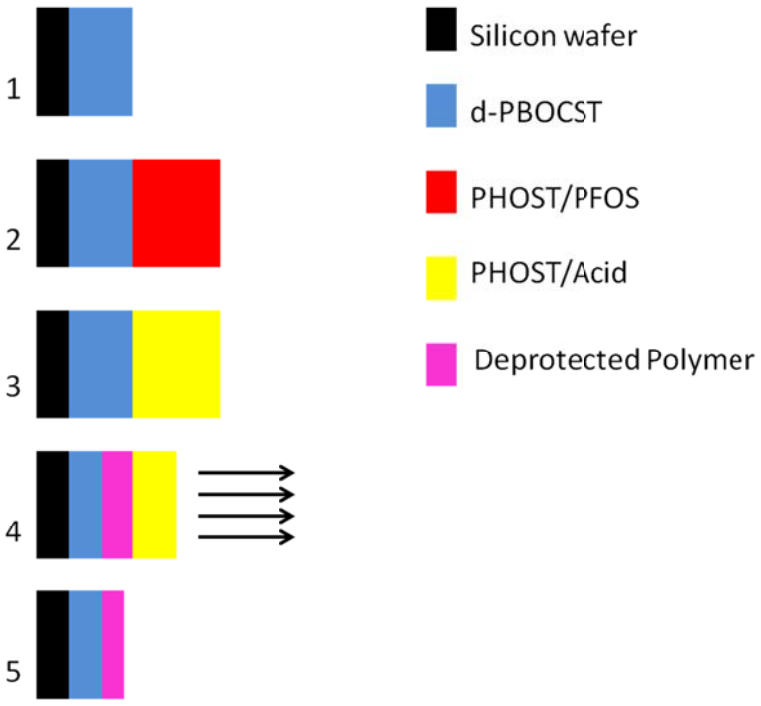

Figure 12. Schematic for Bilayer experiment done by Lin et al.

Trilayer Experiments

Most of the single layer and bilayer studies did not directly measure acid diffusion, but inferred the rates from changes in composition or conductivity. The trilayer technique is a bit more direct in that it measures the time required for a catalyst to traverse a film of known thickness. The trilayer technique is a bit more direct in that it measures the time required for a catalyst to traverse a film of known thickness. As shown before in Figure 9, the bottom layer is an acid feeder layer. The middle layer is a polymer of known thickness. The top layer is the detector layer.

Postnikov et al. used poly(*t*-butyloxycarbonyloxystyrene) (*t*-BOC) as the detector layer that would convert to poly(4-hydroxystyrene) (PHS) once the acid reached there. They monitored the reaction using FTIR by observing the carbonate carbonyl stretch. In theory, it is possible to prepare a trilayer by spin-coating each layer on top of the previous layer using "orthogonal solvents", meaning solvents that will not dissolve the coatings already on the substrate. However, it is hard to find such solvents; therefore, a film float method was used to prepare the trilayer film. In this method, the second and third layers are first spin-coated onto a glass substrate then floated on top of water (similar to Step 3 in Figure 11). Each layer is sequentially picked up using the same silicon wafer. Unfortunately, no diffusion was detected through PHS using this technique and they attributed it to the fact that PHS has a T_g value of 180 °C, too high for temperatures used in lithographic applications and for acid to traverse through[19]. However, the PHS layer was ~100 nm thick, likely much larger than the acid diffusion length over the time scale of the experiment.

Stewart et al. used the same floating method to produce a trilayer with poly(4-isopropyloxycarbonyloxystyrene) (IPOCST) or poly(4-neopentyloxycarbonyloxystyrene) (NPOCST) as the middle layer, meaning the polymer under investigation. NPOCST was used for the acid detection layer, and Poly(4-methoxystyrene) (PMOS) with bis(4-*t*-butylphenyl)iodonium perfluorobutane-1-sulfonate (Nonaflate PAG) was used for an acid feeder layer. Measuring reaction-diffusion in IPOCST and NPOCST provides insight into the more complicated and relevant processes of PBOCST, as IPOCST and NPOCST are similar in structure to PBOCST but unreactive to the diffusing acid catalyst. Therefore, Stewart et al. describe an experiment that separates reaction effects from catalyst diffusion effects.

The diffusion coefficient is calculated assuming Fickian transport,

$$D = \mathrm{L}^2/2\mathrm{t}_{\mathrm{diffusion}}, \tag{3}$$

where D is the diffusion coefficient, L is the thickness of the intermediate layer, and $t_{diffusion}$ is the time it takes for the catalyst to reach the detector layer[23]. It was reasonable to use a Fickian diffusion model since the polymer environment is unreactive to the acid movement.

The trilayer schematic is shown below in Figure 13. The acid feeder layer is spincoated on a silicon wafer first. It consists of PMOS and Nonaflate. The remaining layers were stacked using the film float method. The intermediate layer was either IPOCST or NPOCST. The acid detector layer on top was PBOCST.

Figure 13. Polymer film stack used to measure diffusion rates.

IPOCST and NOPCST are close in chemical properties to TBOCST except that they require a much stronger acid than nonaflate to react. Table 2 summarizes the diffusion coefficients measured at temperatures near their glass transition. T_g for IPOCST and NPOCST are 88 °C and 82 °C, respectively. The deprotection reactions were done for 65 – 95 °C (IPOCST) and 70 – 95 °C (NPOCST) temperature range.

Table 2. Diffusion coefficients near glass transition temperature.

$T-T_g$ (°C)	D (cm^2/s) IPOCST	D (cm^2/s) NPOCST
10	-	6.1×10^{-12}
5	3.7×10^{-12}	1.4×10^{-12}
0	2.7×10^{-12}	6.0×10^{-13}
-5	1.6×10^{-12}	2.0×10^{-13}
-10	3.5×10^{-13}	9.2×10^{-14}
-15	1.3×10^{-13}	2.5×10^{-14}
-20	8.8×10^{-14}	-

Even though NPOCST has a glass transition temperature below that of IPOCST, the diffusion coefficients for NPOCST are smaller as compared to that of IPOCST, at every temperature. Other studies have shown diffusion coefficients for similar polymer

resists. IBM researchers estimated a range of 5×10^{-16} cm^2/s at 65 °C to 1.5×10^{-13} cm^2/s at 105 °C for Nonaflate in TBOCST. At the point of overlap in the two data sets, *D* estimate for IPOCST is 1.3×10^{-13} cm^2/s. For PFOS acid, which is a larger molecule than nonaflate, the *D* estimate reflect this as the range for PFOS is 2.6×10^{-16} cm^2/s at 90 °C to 1×10^{-14} cm^2/s at 130 °C, approximately two orders of magnitude smaller than Nonaflate[23]. The next section explores the kinetics model used in this project.

Acid catalyzed deprotection kinetics model

Earlier investigations assumed that the acid-catalyzed reaction rate follows first order kinetics in acid and reactant concentrations[24–26]. However, these models could not capture the measured kinetics in these systems. Wallraff et al. studied acid catalyzed deprotection kinetics in resist materials using Infrared absorbance spectroscopy. The author(s) assumed that using high concentrations of acid would make acid diffusion insignificant. However, the model deviated from experimental data and they were unable to explain this deviation[24]. Zuniga and Neureuther reported a non-linear dependence of deprotection rates on acid concentration in experimental data[27], which could not be explained by a first-order kinetics model. Therefore, more recent studies aimed to incorporate acid diffusion into models for deprotection kinetics. Postnikov studied photoacid diffusion in a bilayer system and observed there was a fast initial diffusion rate that slowed to a negligible rate after a couple of minutes. Also, increasing the acid concentration above a certain value had negligible effect on the path length. These observations confirmed non- Fickian diffusion[19].

Kang et al. observed that increasing fractions of inert monomer units in the polymer reduced the photoacid transport rate measured with infrared spectroscopy. They

also noted that deprotection rates were slower at longer times. They interpreted these behaviors as acid trapping. The photoacid is a strong hydrogen bond donor while the phenol (inert monomer) and the carboxylic acid (deprotected monomer) groups on the polymer backbone are hydrogen bond acceptors. Such interactions lower the diffusion rate of the photoacid and the overall reaction rate, which is controlled by acid diffusion. They modeled this behavior by using a constant acid diffusivity, but adding an acid trapping reaction that is first order in concentration of acid and deprotected sites[28,29].

This phenomenological model is described by the following system of differential equations, in one dimension for simplicity:

$$\frac{d\phi(x,t)}{dt} = K_P * (1 - \phi) * H(x,t) \text{ and} \quad (4)$$

$$\frac{dH(x,t)}{dt} = D * \frac{d^2H(x,t)}{dx^2} - K_T * H(x,t) * \phi(x,t), \quad (5)$$

where, $\phi(x,t)$ is the instantaneous deprotection level, $H(x,t)$ is the instantaneous acid concentration, D is the acid diffusivity, and $-K_P$ and K_T are the reaction rates for deprotection and trapping, respectively[5].

This model assumes that the by-product is inert. It does capture the long time behavior in real photoresist systems, but underestimates the conversion at short times that are relevant for semiconductor lithography. Equations (4) and (5) have been used to model the measured deprotection rates in bulk films with infrared absorbance spectroscopy. Bulk films have active acid catalyst throughout the volume of the material, so there is no macroscale gradient in acid concentration. Therefore, the governing equations are:

$$\frac{d\phi(t)}{dt} = K_P * (1 - \phi) * H(t) \text{ and} \quad (6)$$

$$\frac{dH(t)}{dt} = -K_T * H(t) * \phi(t) , \quad (7)$$

where K_p is the apparent acid catalysis reaction rate constant and K_T is the apparent trapping rate for the acid. At high deprotection levels, the trapping effect is stronger[29]. Kang et al. considered a first order dependence on the extent of the reaction to consider trapping of acid by deprotection products as a primary physical mechanism. The temperature dependence of the reaction rates is given by the Arrhenius equation

$$\ln K_P = A - \frac{E_a}{RT} , \quad (8)$$

which is used to determine the activation energy E_a and the prefactor, *A*. A higher activation energy implies that the reaction rate is more sensitive to temperature. Also, a lower T_g should lead to higher K_p and K_T values. The barriers to diffusion are reduced when the temperatures are close to T_g because the chains in the polymer matrix start gaining mobility[29]. One would expect diffusion to increase at temperatures above T_g due to higher mobility of polymer chains.

The next chapters discuss the use of Infrared Absorbance Spectroscopy to measure deprotection rates. These data are fit using equations (6) and (7) to obtain K_P and K_T parameter values. These studies illustrate the failing of this model to capture short-time behavior. Future work will incorporate non-Fickian transport model to capture the behavior over all time scales.

CHAPTER 3: INFRARED SPECTROSCOPY

The goal of this project is to measure deprotection kinetics in thin films of chemically amplified resists. The variable parameters include reaction temperature, catalyst loading, and catalyst type [30,31].

Materials

The polymer resin used was poly(4-hydroxystyrene-co-tert-butyl acrylate-co-styrene), hereafter referred to as PHOST-PtBA-PS, provided by DuPont Electronic Polymers. This terpolymer has a weight-average molecular weight of 11.7 kg/mol, dispersity of 2.0, and a molar ratio of 59.5/20.7/19.8 for HOST, tBA, S, respectively. The 4 homopolymers used in this project were PHOST, PtBA, PS and polyacrylic acid (PAA). These homopolymers were bought from Sigma Aldrich and had a weight-average molecular weight of 11 kg/mol, 13 kg/mol, 5 kg/mol, 450kg/mol, respectively. The two photoacid catalysts used were triphenylsulfonium triflate (PAG1, M_w = 412.45 g/mol) and triphenylsulfonium perfluoro-1-butanesulfonate (PAG2, M_w = 562.47 g/mol), both bought from Sigma Aldrich as well. Propylene glycol monomethyl ether acetate (PGMEA, M_w = 132.16 g/mol) was used as the solvent. The terpolymer film was spincoated on a double sided polished p-type (100) high resistivity (>6000 Ω) silicon wafer to avoid the dopant peak at 1107 cm^{-1} in the IR spectra.

Reactions

The deprotection reaction occurs in two steps. First, the photoacid catalyst is activated using UV light to produce the photoacid, as shown in Figure 14a) and Figure 14b). When the polymer film is heated the photoacid deprotects the terpolymer by

cleaving the C-O bond of tert-butyl acrylate to produce acrylic acid, shown in Figure 14c). In the process, the photoacid is regenerated and cause another deprotection event.

a)

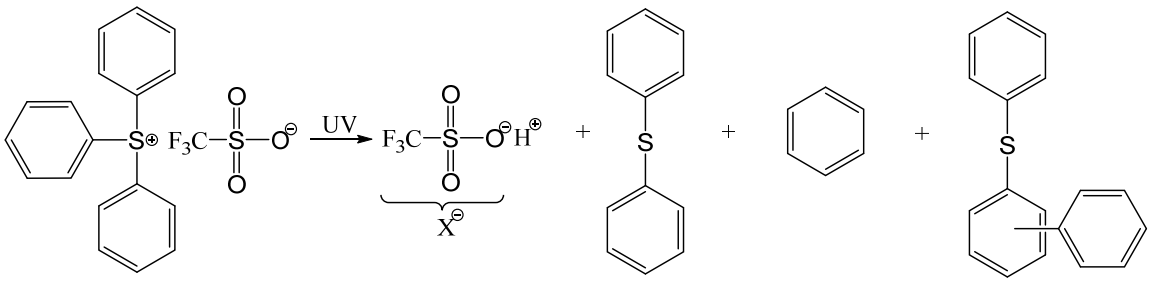

b)

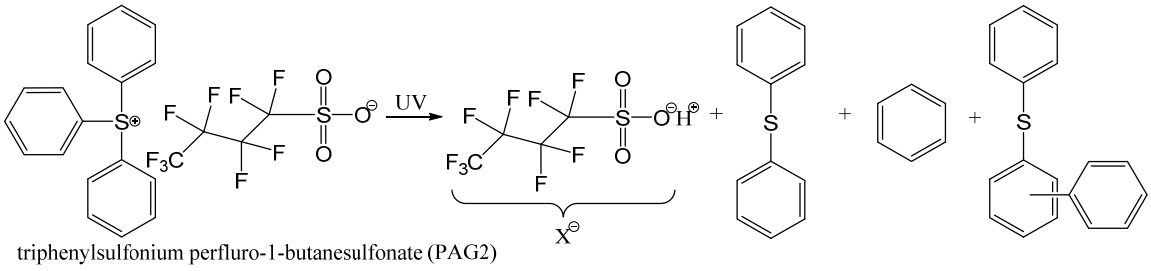

c)

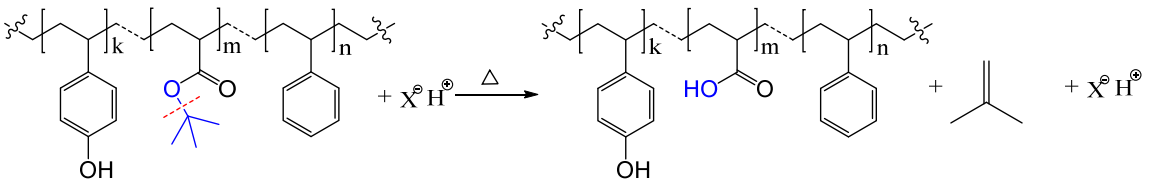

Figure 14. Reaction scheme for a) small acid generation[31,32] b) bulky acid generation[31,32] c) Deprotection reaction between polymer and photoacid[31,32].

An FTIR (Fourier Transform Infrared spectroscopy) instrument was used to monitor the cleaving of C-O bond as a function of time. The frequencies (wavelengths) of infrared radiation that are absorbed by the polymer reflect the vibrational energies of different chemical bonds. An FTIR produces an interferogram by recording the relative amount of radiation that reaches the detector after passing through the sample (gases, liquids, or solids). The computer reads the interferogram and uses Fourier Transform to decode the radiation intensity information for each wavelength and produces the final absorbance spectrum as a function of wavenumber (inverse of wavelength)[33]. A Nicolet 6700 FT-IR spectrometer was used in this project to monitor the deprotection reaction as a function of time.

Since the reacted terpolymer has four different types of monomer units, it was imperative to ensure that the peaks chosen to be monitored were unique to the reactant or product. Therefore, IR spectra were recorded for the four homopolymers (PHOST, PtBA, PS, PAA) and their characteristic peaks were labeled, shown in Figure 15 to Figure 18. The IR spectrum for unreacted PHOST-PtBA-PS is shown in Figure 19 for comparison, and peaks were assigned based on the reference data. Finally,

Table 3 summarizes the peak assignments for the 4 reference homopolymers along with their origination[34].

Based on the information gathered from these spectra, two peaks were chosen to be monitored, 1150 cm^{-1} and 1170 cm^{-1}. The 1150 peak was chosen because it corresponded to the cleaving of C-O bond in the tert-butyl acrylate. The 1170 cm^{-1} peak, originating from HOST, is constant throughout the reaction and used as a reference peak to account for density changes in the polymer films due to deprotection. The other peaks, from inert monomers in the reaction, were difficult to monitor since they appeared in the fingerprint region (600 cm^{-1} to 1400 cm^{-1}) of the IR spectra[34,35].

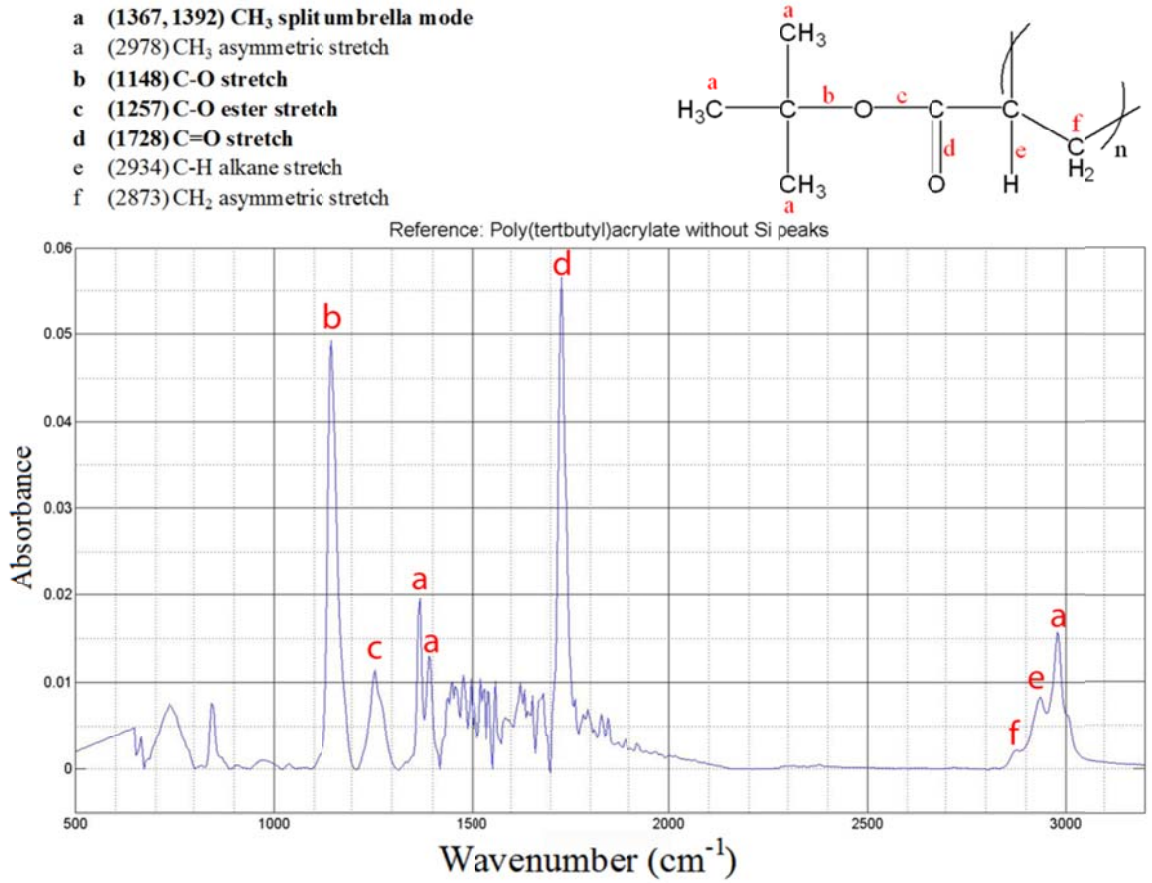

Figure 15. IR spectrum of poly(tert-butyl acrylate) (PtBA)

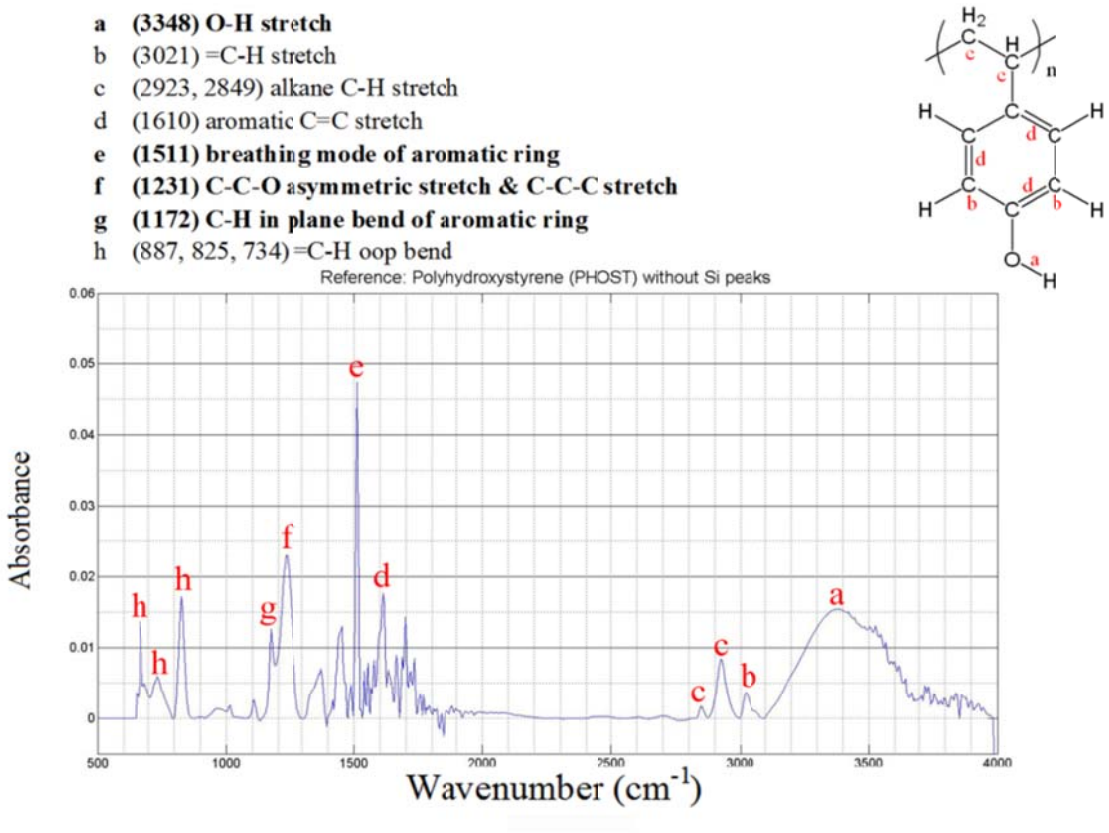

Figure 16. IR spectrum of poly(4-hydroxystyrene) (PHOST)

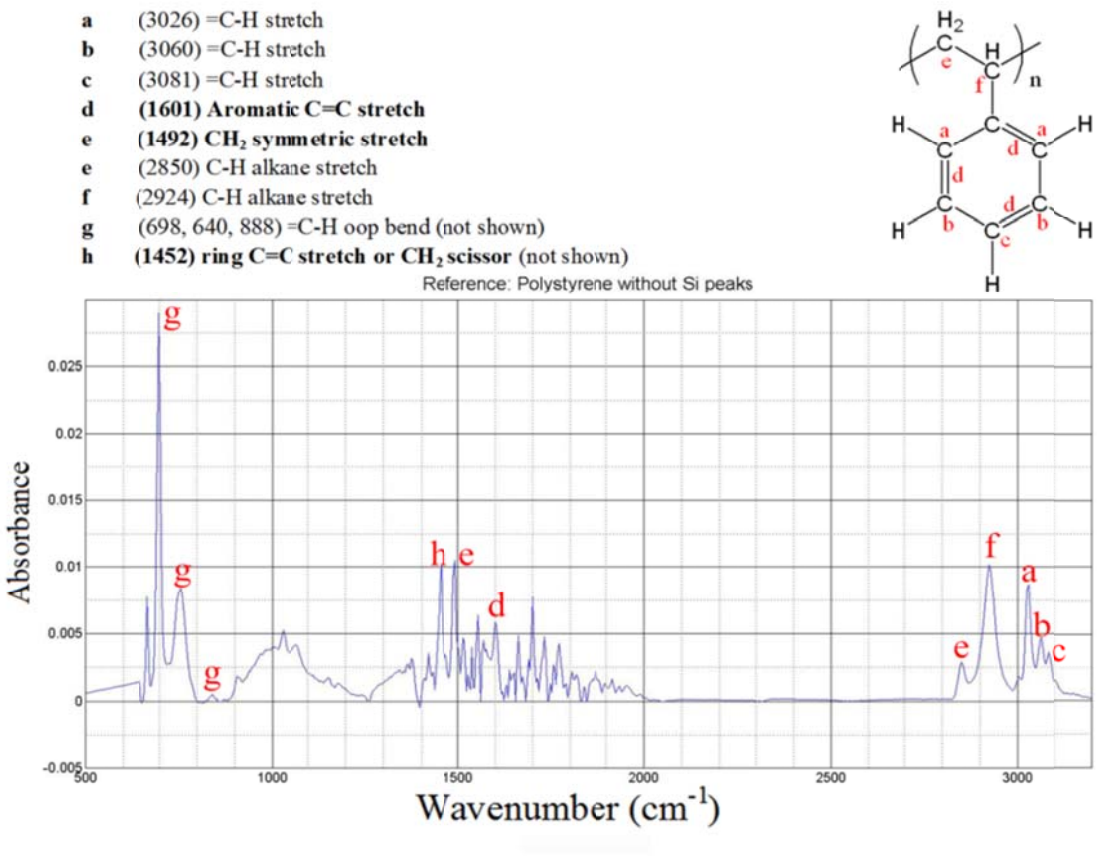

Figure 17. IR spectrum of Polystyrene (PS)

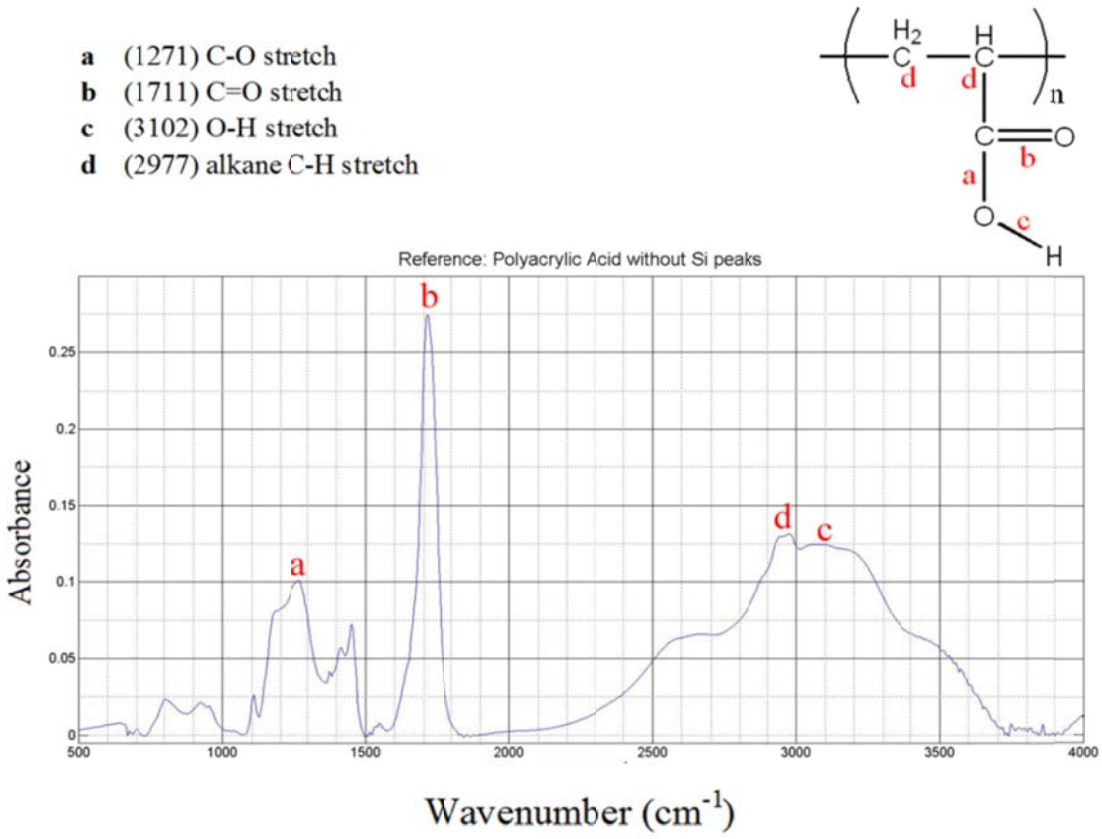

Figure 18. IR spectrum of polyacrylic acid (PAA)

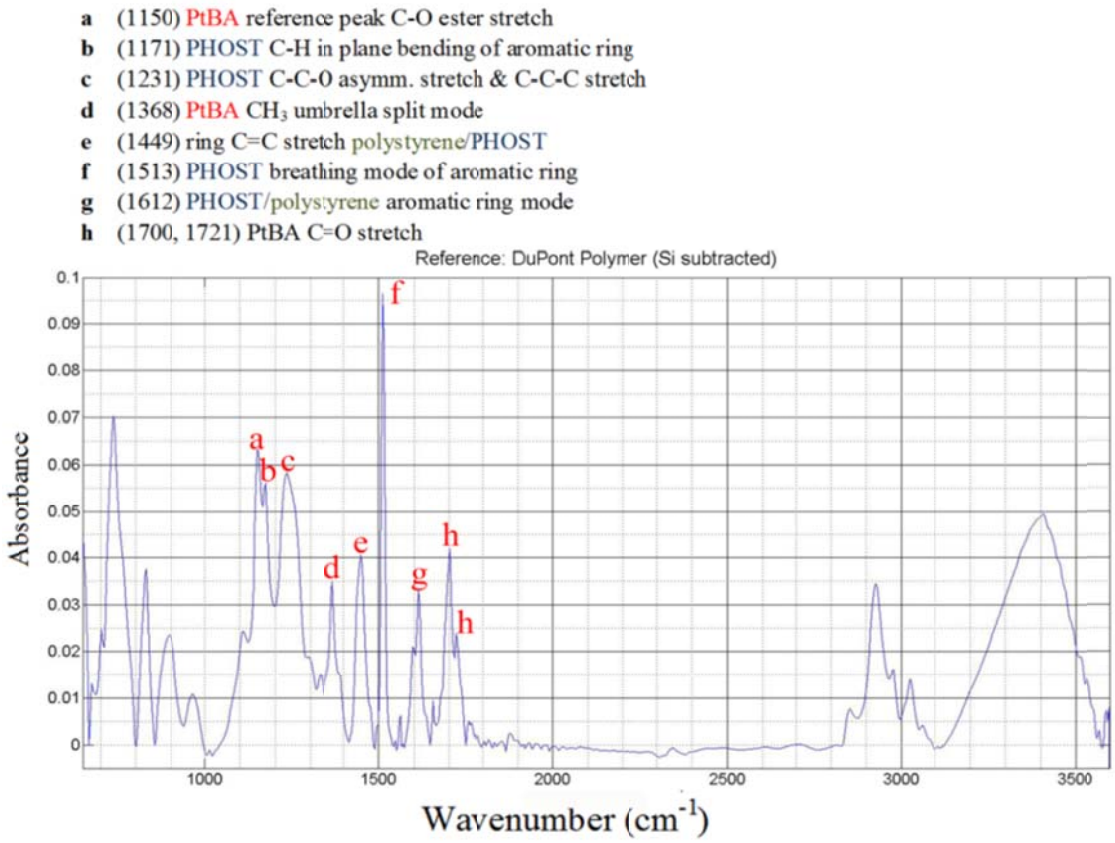

Figure 19. IR spectrum of terpolymer with labeled characteristic peaks from each monomer moiety.

Table 3. IR peak assignments for 4 homopolymers[31,35]

Wavenumber (cm^{-1})	Parent Polymer	Description
1148	PtBA	C-O ester stretch
1172	PHOST	C-H in plane bend aromatic ring
1231	PHOST	C-C-O asymmetric stretch & C-C-C stretch
1257	PtBA	C-O ester stretch
1271	Polyacrylic acid	C-O stretch
1367, 1392	PtBA	CH_3 split umbrella mode
1452	PHOST/Polystyrene	ring C=C stretch or CH_2 scissor
1492	PHOST/Polystyrene	CH_2 symmetric stretch (weak in PHOST)
1511	PHOST/Polystyrene	breathing mode of aromatic ring (weak in Polystyrene)
1601	Polystyrene	Aromatic C=C stretch
1610	PHOST	Aromatic C=C stretch
1711	Polyacrylic acid	C=O stretch
1728	PtBA	C=O stretch

Sample Preparation

The first step in sample preparation is making the polymer-catalyst solution in PGMEA. The polymer was weighed in an amber vial and then left overnight in a vacuum oven at 40 ℃ to remove any water from it. In another amber vial, PAG was weighed and then added to polymer containing vial. In a third vial, PGMEA was weighed and then transferred to the vial containing polymer and catalyst using a pipette. Once everything was dissolved, the solution was filtered using a 1 μm PTFE filter to remove any

particulates unseen to the naked eye. Next, the organic contaminants on the high resistivity silicon wafer were eliminated by using a plasma cleaner (Harrick's Plasma's Basic Plasma Cleaner). Using a spincoater (Brewer Science), a thin film (~250 nm) was casted on the clean silicon wafer. The sample was then soft baked at 130℃ for 4 minutes to eliminate any residual solvent, reducing the thickness of the film to ~230 nm. Finally, the catalyst was activated with a dose of 135 mJ/cm^2 using a 254 nm wavelength ultraviolet lamp. The UV lamp intensity was measured around 5 mW/cm^2 using a UVP Radiometer. The sample preparation is done under orange light that blocks UV wavelengths and prevents activation of PAG.

Using FTIR

FTIR is used to monitor the deprotection reaction by recording absorbance vs. time. The FTIR is equipped with a customized heat cell in the loading chamber (shown in Figure 8). The sample is placed in the heat cell and secured using two clips to ensure even heating. A PID controller maintains the set temperature within $\pm$ 2 ℃. For each temperature setting and catalyst loading, a separate macro was written that continuously recorded the IR scans at fixed intervals of time. Each macro consisted of a background collection without the sample in the heat cell, then a quick scan with the sample in the heat cell which served as a reference scan (time = 0 s) for data analysis. IR scans was recorded at a resolution of 8 cm^{-1}. Automated data acquisition provided in-situ measurements that lead to smooth deprotection curves. Deprotection level is defined as the fraction of tBA converted to AA. An overview of how IR scans are converted to deprotection curves is shown in Figure 20. The baseline is calculated for each IR scan using a “point-and-click” method in MATLAB. The $1150cm^{-1}$ and $1170cm^{-1}$ peaks are

fitted to the sum of two Gaussian functions, and the area under each peak is calculated as a function of time. Equation (1) calculates the deprotection level, ϕ, from the area under the two peaks, assuming there are no deprotected sites when the first scan is required. Figure 7 shows deprotection level vs. time for 3 runs at 80℃ with PAG1 ($2.41x10^{-2}$ nm^{-3})

$$\phi = 1 - \frac{Area_{1150,t}}{Area_{1150,t=0}} * \frac{Area_{1170,t=0}}{Area_{1170,t}}, \quad (9)$$

where $Area_{1150,t}$ and $Area_{1170,t}$ are areas under peak 1150 cm^{-1} and 1170 cm^{-1} at time t, respectively.

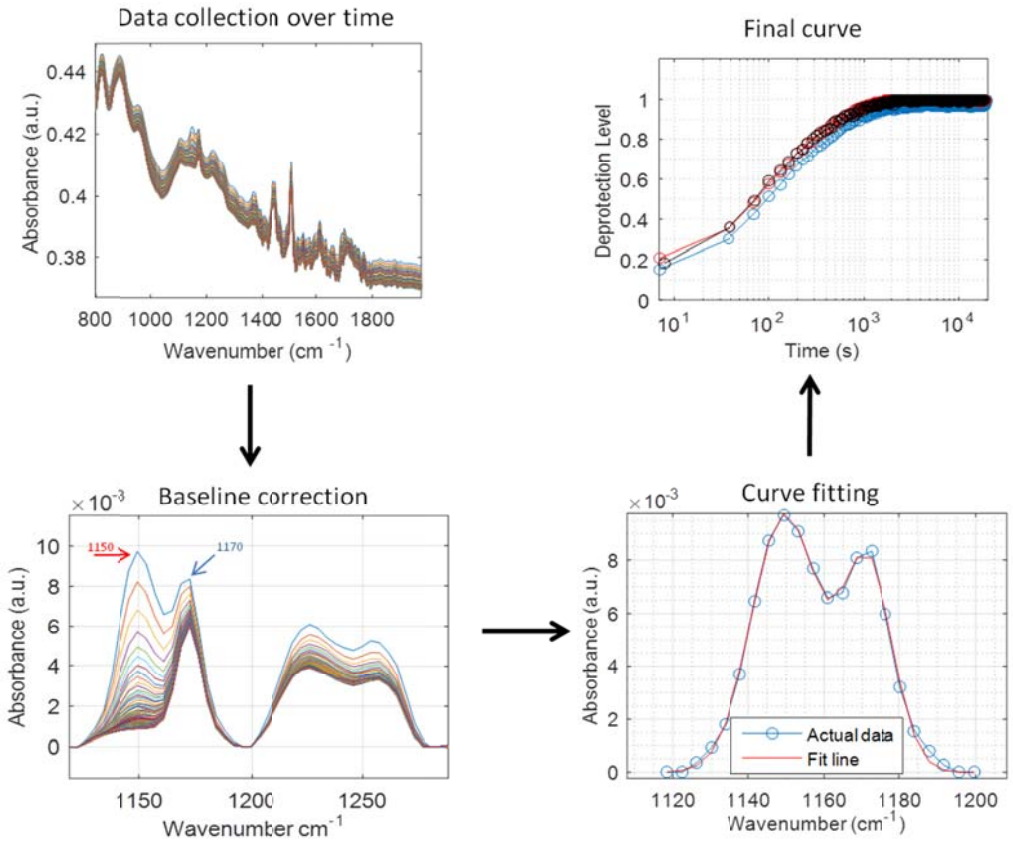

Figure 20. Flowchart showing how raw data from the FTIR is converted to Deprotection level vs. time curve.

Table 2 shows the different temperature and catalyst loadings at which IR scans were collected for each of the two photoacid catalysts. Tables also show whether the experiments were reproducible or not.

Table 4. Summary of reactions that were reproducible or not for Triflate.

Triflate concentration	**65℃**	**70℃**	**75℃**	**80℃**
2.41×10^{-2} nm^{-3}	Not reproducible	Not reproducible	Reproducible	Reproducible
6.42×10^{-2} nm^{-3}	Not reproducible	Reproducible	Reproducible	Reproducible
11.2×10^{-2} nm^{-3}	Reproducible	Reproducible	Reproducible	Reproducible
14.5×10^{-2} nm^{-3}	Reproducible	Reproducible	Reproducible	Reproducible

Table 5. Summary of reactions that were reproducible or not for PFBS.

PFBS concentration	**70℃**	**75℃**	**80℃**	**85℃**
2.41×10^{-2} nm^{-3}	N/A	N/A	N/A	Not reproducible
6.42×10^{-2} nm^{-3}	Reproducible	Reproducible	Reproducible	Reproducible
11.2×10^{-2} nm^{-3}	Reproducible	Reproducible	Reproducible	Reproducible
14.5×10^{-2} nm^{-3}	Reproducible	Reproducible	Reproducible	Reproducible

Each experiment was repeated at least three times to ensure reproducibility. For triflate, the deprotection data at low temperature and low concentration (65℃, 70℃ and 2.41×10^{-2} nm^{-3}) were not reproducible. For PFBS, 85℃ and 2.41×10^{-2} nm^{-3} was not reproducible therefore lower temperatures were not tested.

CHAPTER 4: RESULTS AND DISCUSSION

This chapter presents deprotection rates measured by infrared absorbance spectroscopy as a function of temperature, acid catalyst concentration, and acid catalyst size (controlled by the type of counterion). First, measurements with inactive catalyst confirm there is no thermal deprotection over the temperature range of interest. Second, data are presented that suggest deprotection rates are controlled by the reaction at very short times, but after initial deprotection events the rates are controlled by mobility of the acid-counterion pair. Finally, data are fit to a simple model to extract apparent rate constants for deprotection (K_p) and acid loss (K_t). The activation energy for deprotection is consistent with reported values for diffusion controlled reactions in polymers.

Inactive Catalyst

The highest temperature used for the reactions was 85 °C. It was important to check whether the reaction could occur without active catalyst. Figure 21 compares the IR spectrum when the sample is heated from room temperature to 85 °C with active and inactive 14.5×10^{-2} nm^{-3} catalyst. It is clear that when the catalyst is not active, no reaction occurs since the C-O stretch peak remains unchanged.

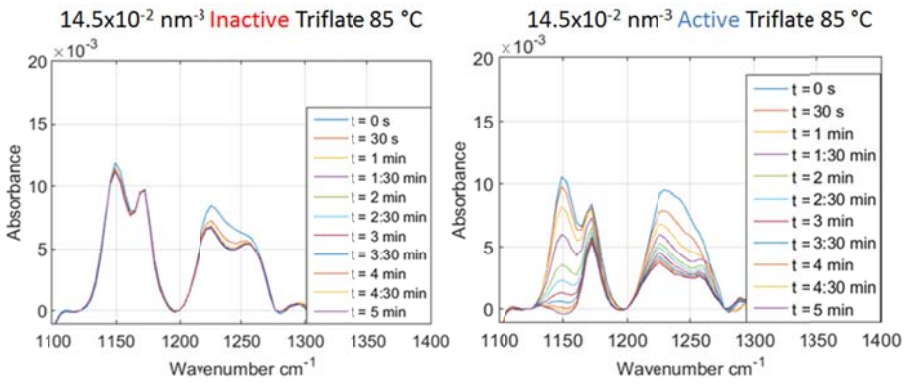

Figure 21. Comparison of active and inactive catalyst when heated from 25 °C to 85 °C.

The reaction kinetics was also measured under non-isothermal conditions, to see if deprotection is likely to occur when the sample first makes contact with the stage. This is important because it requires approximately 10 sec to load the sample and acquire the first scan. Figure 22 demonstrates that a deprotection extent of 0.0167 is detected when the stage temperature reaches 28 °C, which suggests that the first IR measurement will capture a state with some initial level of deprotection that is set by the temperature and catalyst loading.

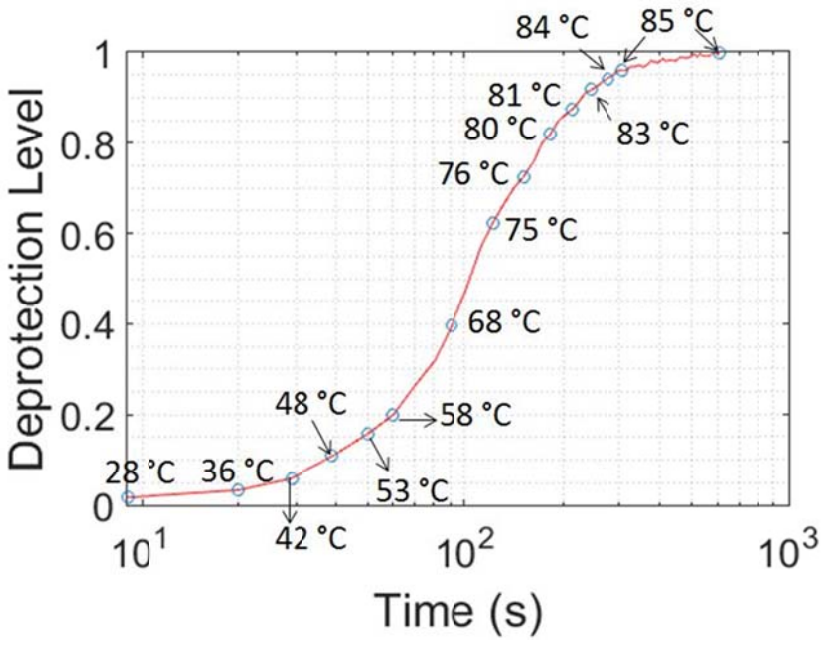

Figure 22. Deprotection level for 14.5×10^{-2} nm^{-3} active triflate vs. temperature and time.

Kinetics at low temperature

To better understand the initial deprotection level, the next experiment measures the kinetics at low temperature. In these tests the sample is loaded on the pre-heated stage at 40 °C, and then data are recorded as a function of time. The reaction is activated at the low temperature, although it is very slow. Figure 23 reports these data for two different

catalysts at 40 °C. The initial deprotection rates are similar for the two catalysts, but beyond a deprotection level of approximately 0.1 the larger PFBS counterion exhibits slower kinetics than triflate. These data suggest that initial deprotection rates are reaction-controlled, while slow diffusion limits the deprotection rates at longer time scales: If each acid catalyst deprotects a tBA group, then the initial deprotection level with 14.5×10^{-2} nm^{-3} should be 0.13, which is consistent with the observed behavior. After the deprotection reaction, the acid must diffuse to a new site to catalyze a new reaction, and this process is sensitive to the size of the acid-counterion pair (a free volume effect). Therefore, we propose that IR data for higher temperature should be corrected for an "instantaneous deprotection" that is set by the catalyst concentration.

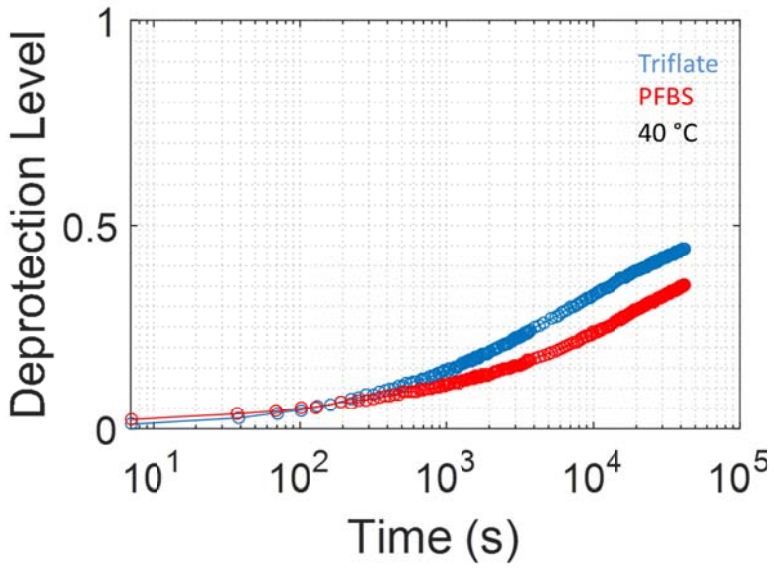

Figure 23. Deprotection Level vs. time for PFBS and triflate at 40 °C.

Initial Deprotection Level Calculations

Deprotection level vs. time was measured for a temperature range of 65 °C to 85 °C for triflate and 70 °C to 85 °C for PFBS in increments of 5 °C. It was observed that

there was instantaneous deprotection as soon as the sample came into contact with the heat cell. Based on these outcomes, Equation 9 was modified to include an instantaneous deprotection instead of assuming that no reaction occurs at time t = 0 sec. In order to modify the equation, first the total number of active sites (tBA) per nm^3 were calculated using the acid concentration. The following equation was used to calculate the total number of tBA sites per nm^3. The number of tBA sites per nm^3 (n_{tBA}) is given by Equation 10,

$$n_{tBA} = f_{tBA} * \frac{\rho}{M_0} * N_A * 10^{-21}, \quad (10)$$

where f_{tBA} = 0.198, is the fraction of tBA site in the polymer, ρ = 1.1g/cm^3, is the density of the polymer, M_0 = 118 g/mol is the molecular weight of the polymer, and N_A is the Avogadro's number in mol^{-1}.The acid concentration was calculated using Equation 11,

$$H_0 = w_{PAG} * \frac{\rho}{M_{PAG}} * N_A * 10^{-21}, \quad (11)$$

where, H_0 is the initial acid concentration in nm^{-3} and w_{PAG} is the weight fraction of the acid relative to the polymer. We assume that each acid initially deprotects one nearby tBA group, so the initial deprotection level is φ_0. At time t = 0, $\varphi \neq 0$ and there is a need for a rescale which is shown below. Let x be the fraction of instantaneous deprotection tBA sites. Equation 9 is then modified as the following equation,

$$\phi = 1 - \left(\frac{Area_{1150,t}}{Area_{1150,t=0}} * \frac{Area_{1170,t=0}}{Area_{1170,t}}\right) * (1 - \phi_0) . \quad (12)$$

Equation 12 is the modified deprotection level equation that is used to fit the experimental data. The initial deprotection levels for each acid concentration are summarized in Table 6 below.

Table 6. Instantaneous deprotection level for each acid concentration.

Acid concentration (nm^{-3})	**Initial Deprotection Level**
2.41×10^{-2}	0.0219
6.42×10^{-2}	0.058
11.2×10^{-2}	0.102
14.5×10^{-2}	0.131

Modeling Deprotection Rates

The deprotection levels calculated from the IR data were fit to Equations 6 and 7 using a non-linear regression method in MATLAB to extract K_p and K_t values. Figure 22 and Figure 23 show the best fits for 6.42×10^{-2} nm^{-3} acid concentration and predicted profiles using the same set of parameters for the other two acid concentrations. It is observed that the K_p values for each type of PAG steadily increase with temperature, as expected. Also, the K_p values for PFBS are slightly lower than that of triflate at each temperature.

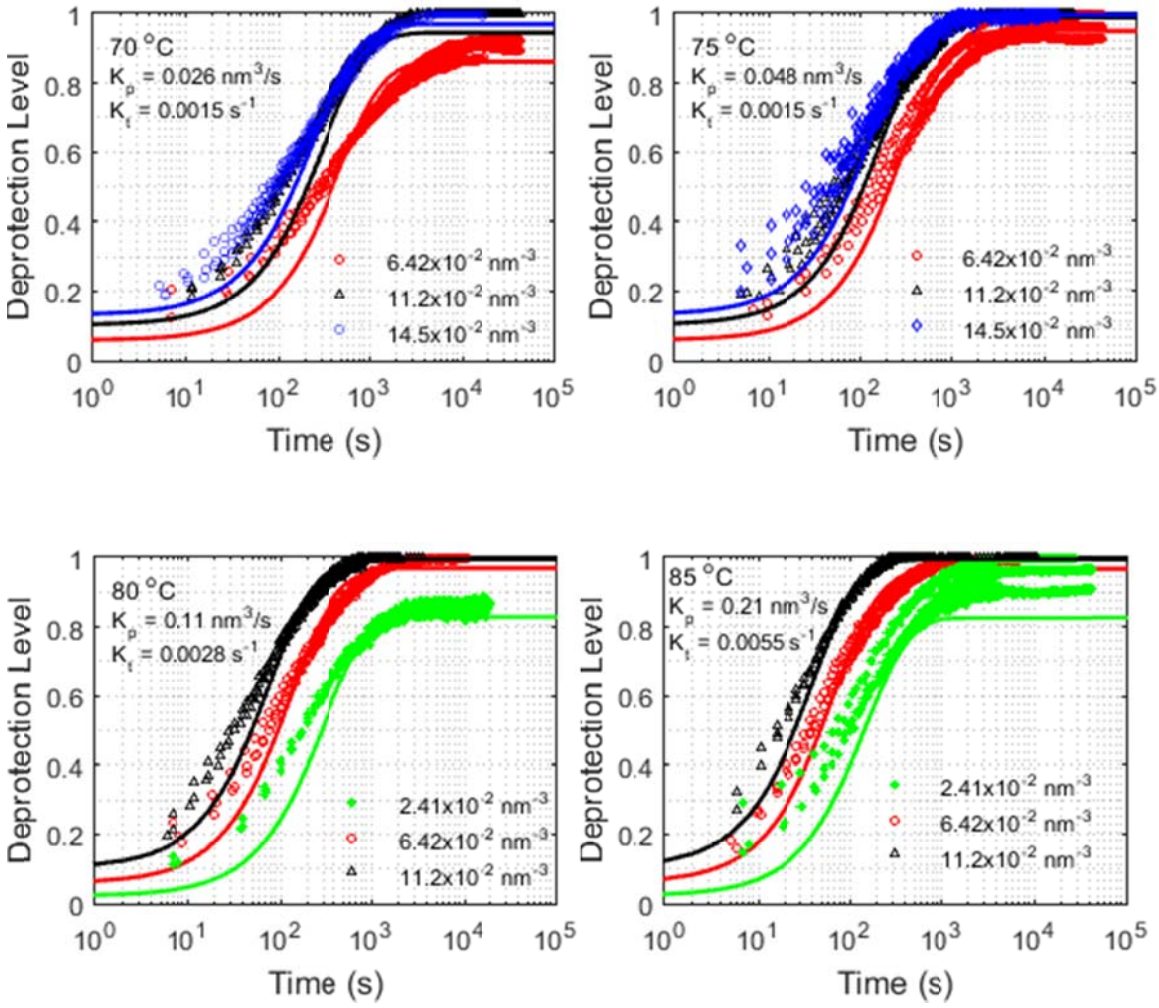

Figure 24. K_p and K_t plots for triflate. Solid lines are predicted profiles basd on best-fit results for an acid concentration of 6.42×10^{-2} nm^{-3}.

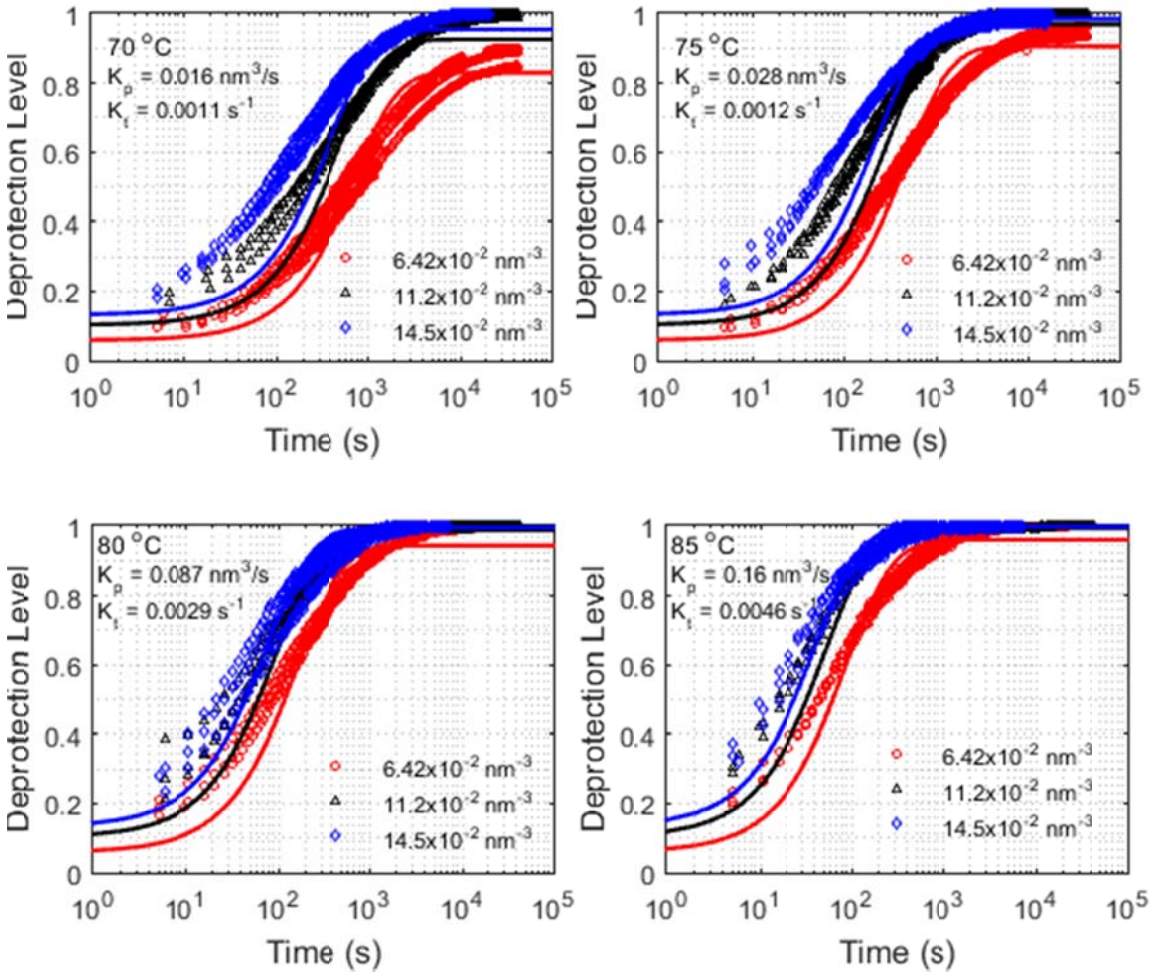

Figure 25. K_p and K_t plots for PFBS. Solid lines are predicted profiles based on best-fit results for an acid concentration of 6.42×10^{-2} nm^{-3}.

Using the K_p values extracted for each temperature, Arrhenius plots were made to extract activation energy and the pre-exponential factor. The plots are shown in Figure 26 and the parameters are summarized in Table 7.

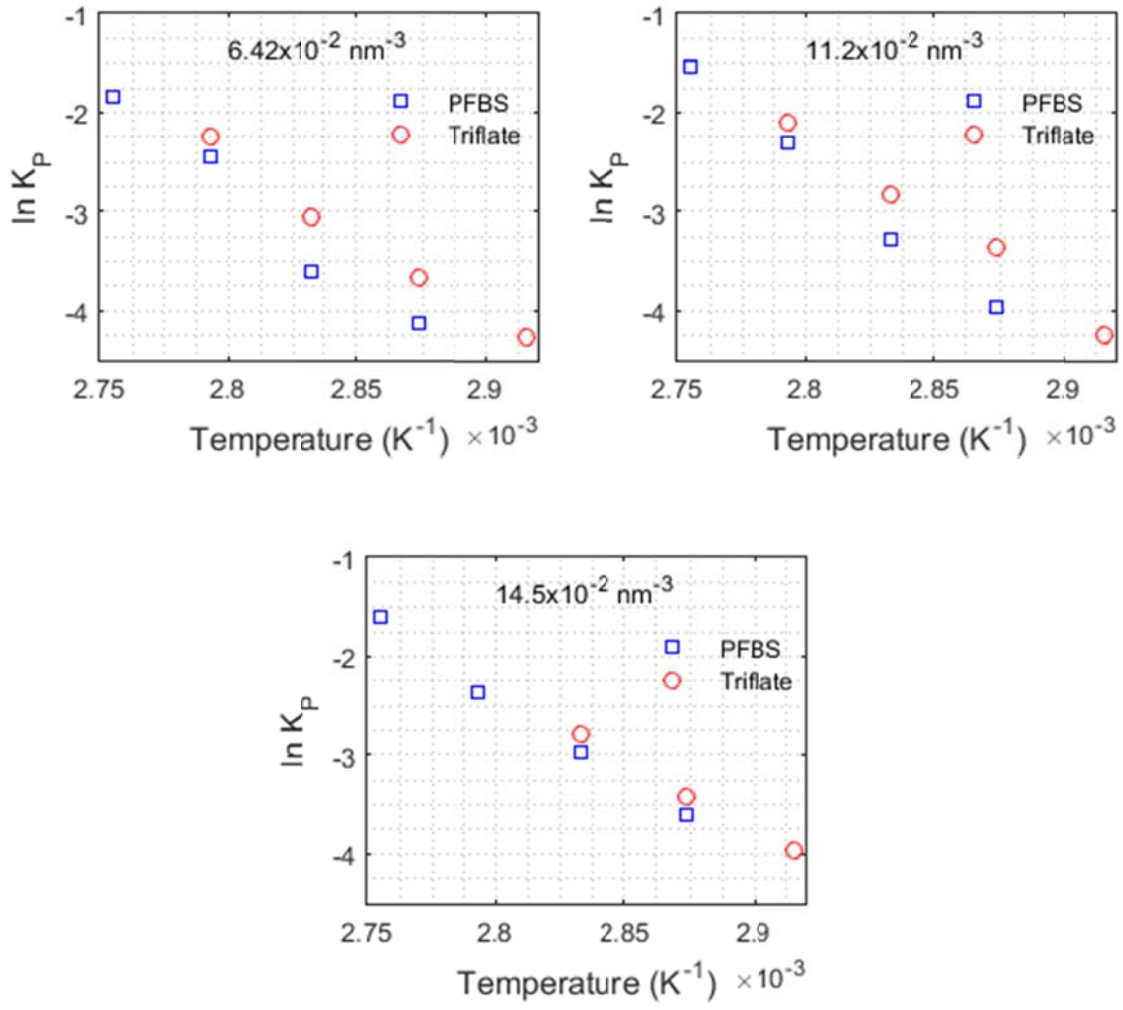

Figure 26. Arrhenius plots for Triflate and PFBS at three acid concentrations.

Table 7. Parameters extracted from Arrhenius plots.

Acid concentration (nm^{-3})		6.42×10^{-2}	11.2×10^{-2}	14.5×10^{-2}
Triflate	E_a (kJ/mol)	137±8	141±9	117±6
	A (cm^2/s)	8.58×10^{18}	5.41×10^{19}	1.04×10^{16}
PFBS	E_a (kJ/mol)	169±18	173±8	138±6
	A (cm^2/s)	3.25×10^{23}	1.84×10^{24}	1.56×10^{19}

Houle et al. calculated activation energies for diffusion in deprotected and protected polymer which ranged from 100 kJ/mol to 152 kJ/mol, respectively for a t-BOC positive photoresist below its T_g value[36]. Wallraff et al. reported activation energy of 137 kJ/mol for reaction in t-BOC[24]. Kang et al. found an activation energy of photoacid diffusion of PFBS in poly(HOST-*co*-tBA) to be around 127 kJ/mol[29]. Fryer et al. observed that the diffusion coefficient and activation energy increased by at least an order of magnitude when PEB temperatures were increased from below T_g to 5 °C above the T_g value of the novolac resin (T_g = 91 °C). Also, the acid acted as a plasticizer for their photoresist system[12], which reduced the activation energy for diffusion.

The activation energies reported in Table 7 are consistent with other studies of acid diffusion in glassy photoresists. The decrease in the activation energy for the highest acid concentration in this project might be explained by the depression of T_g due to acid catalyst. To test for this behavior, the T_g was measured using spectroscopic ellipsometry, a technique that can detect the change in thermal expansion for a polymer glass and polymer melt. The T_g measurements were taken with triflate and PFBS as the acid catalysts. A 250 nm polymer film with the catalyst was spin-coated on silicon wafer. The film was soft baked at 130 °C for 10 minutes before taking T_g measurements. On the Ellipsometer, the temperature was ramped to 160 °C and cooled down to 40 °C at 2 °C/min. Two such cycles were recorded, and the thickness vs. temperature was plotted in Figure 27. The change in slope (thermal expansion) marks the T_g value, which are summarized in Table 8 and Table 9.

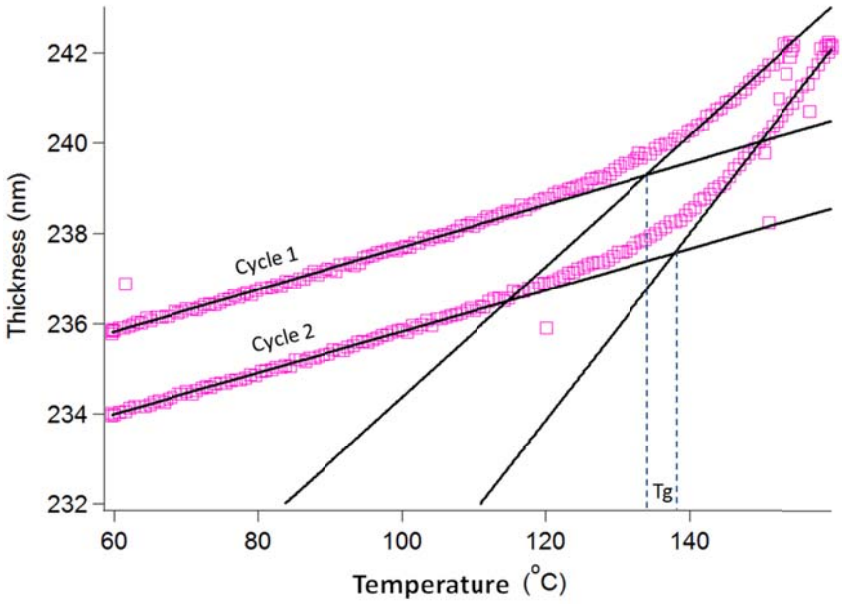

Figure 27. 2 cycles of Tg measurements for polymer with 6.42×10^{-2} nm^{-3} triflate.

Table 8. T_g measurements taken for polymer with different triflate concentrations.

Triflate concentration (nm^{-3})	**T_g (°C) Cycle 1**	**T_g (°C) Cycle 2**
No catalyst/pure polymer	143	143
2.41×10^{-2}	138	140
6.42×10^{-2}	136	137
11.2×10^{-2}	137	136
14.5×10^{-2}	137	137

Table 9. T_g measurements taken for polymer with different triflate concentrations.

PFBS concentration (nm^{-3})	**T_g (°C) Cycle 1**	**T_g (°C) Cycle 2**
No catalyst/pure polymer	143	143
6.42×10^{-2}	137	138
11.2×10^{-2}	137	137
14.5×10^{-2}	136	136

Unfortunately, the decrease in activation energy cannot be explained by the T_g measurements. The acid does act as a plasticizer but the concentration of the acid doesn't really change the T_g value by much. Therefore, the model used to fit the experimental data does not provide a quantitative description and needs to be modified.

CHAPTER 5: FUTURE WORK

By inspection of the data in Figure 24 and Figure 25, it is clear that the first-order reaction coupled to acid loss cannot describe observed kinetics. Industrial lithography processes are implemented over short time scales, typically 1 minute, so capturing the short-time behavior is arguably the most important aspect of any model.

A previous study demonstrated that short-time behavior was captured with a model of fast reaction coupled to a show, non-Fickian diffusion process. This analysis was implemented with spatially-resolved stochastic simulations, and these models will be used to analyze these data in the next phase of this project.

The origin of non-Fickian transport is unclear, and future studies will aim to identify the underlying physical and chemical factors that may contribute to this behavior. One possible explanation is spatial heterogeneities in the glassy polymer resin, which produces regions in the film that are “fast moving” and “slow moving”. Such behavior is difficult to directly measure, but can be inferred from appropriately designed experiments. As an example, the small triflate anion should be less sensitive to such heterogeneities than PFBS, so diffusion should be faster and also closet to Fickian.

It was also speculated that since the reaction is exothermic, local heating could result in a faster rate of reaction which is not accounted for in the kinetics reaction model (i.e., and non-isothermal effects). A dewetting experiment was devised to test for local heating, where the model CA photoresist was coated with an 11 nm film of 4.6kg/mol polystyrene (PS) cast from cyclohexane. The thing film is unstable and will dewet when heated above the glass transition temperature. When the catalyst is not

activated, or if the catalyst is not included in the film, dewetting occurred at 110 °C. Therefore, if heat from the exothermic reaction can elevate the temperature in the film, dewetting should occur at a temperature lower than 110 °C. To test for this behavior, films were loaded with 14.5×10^{-2} nm^{-3} of active. The details of the experiments conducted are summarized in Table 10. triflate was used as the catalyst for these experiments. Figure 28, Figure 29, Figure 30, and Figure 31 show whether dewetting occurs for each of the cases mentioned in Table 10.

Table 10. Dewetting experiments with PS and triflate.

Polymer	**catalyst**	**Temp (°C)**	**Activated**	**Dewetting?**
yes	no	110	N/A	yes
yes	yes	110	no	yes
yes	yes	110	yes, without PS on top	yes
yes	yes	110	yes, with PS on top	No

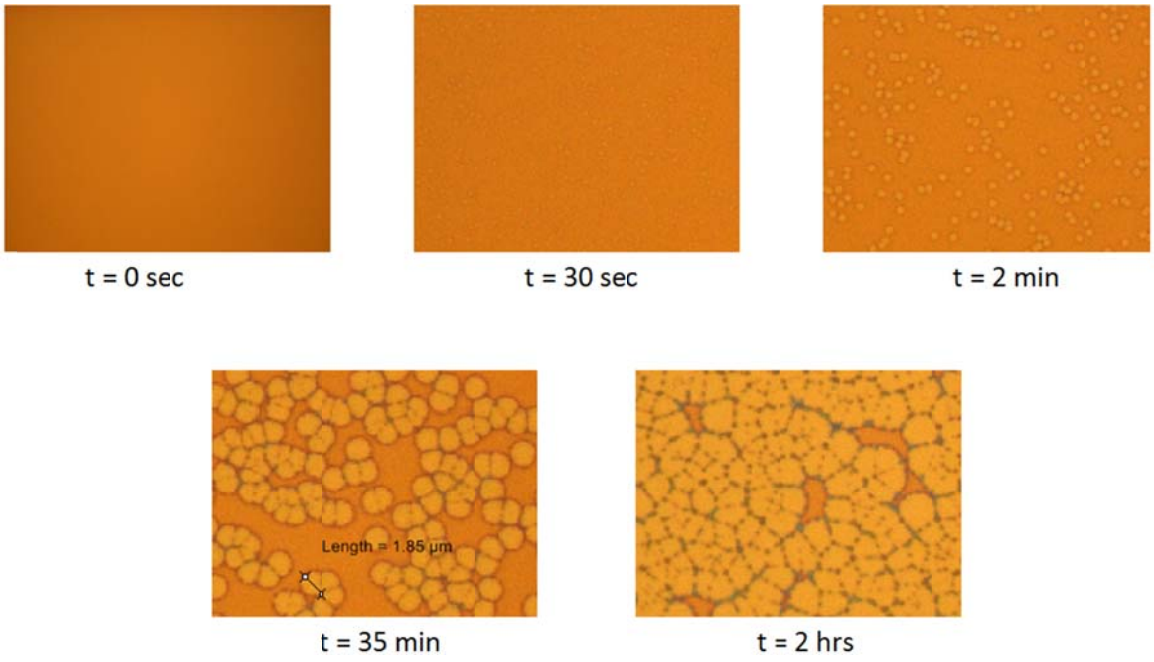

Figure 28. PS film spin-coated on top of a pure polymer film and heated at 110 °C.

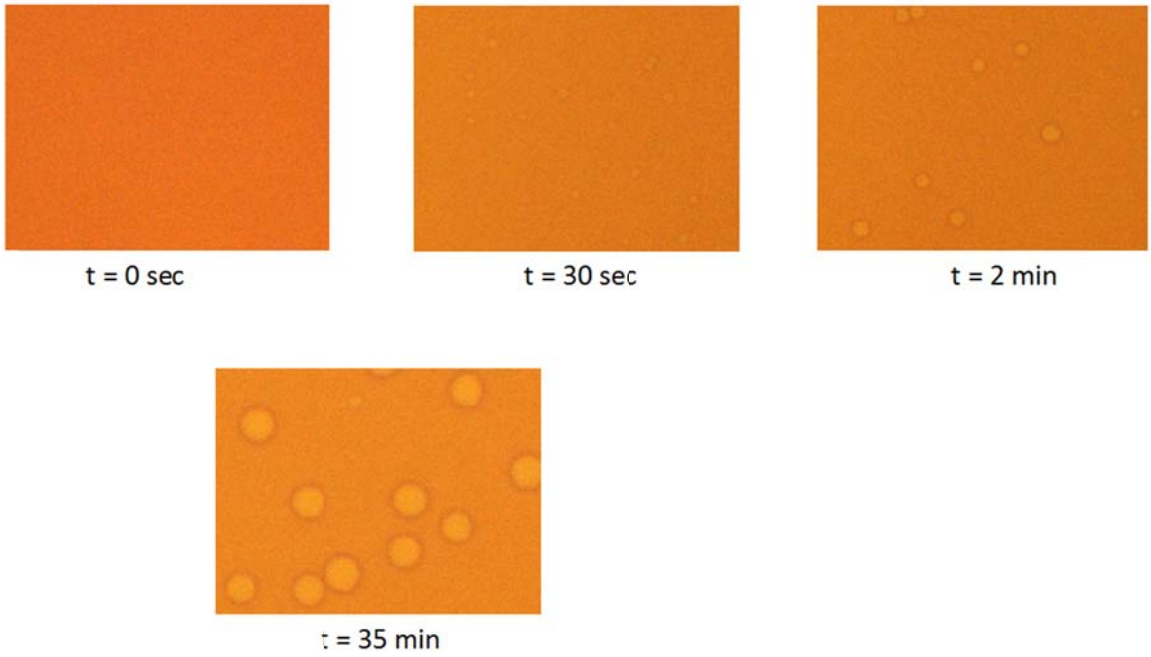

Figure 29. PS film spin-coated on top of a polymer and inactive catalyst and heated.

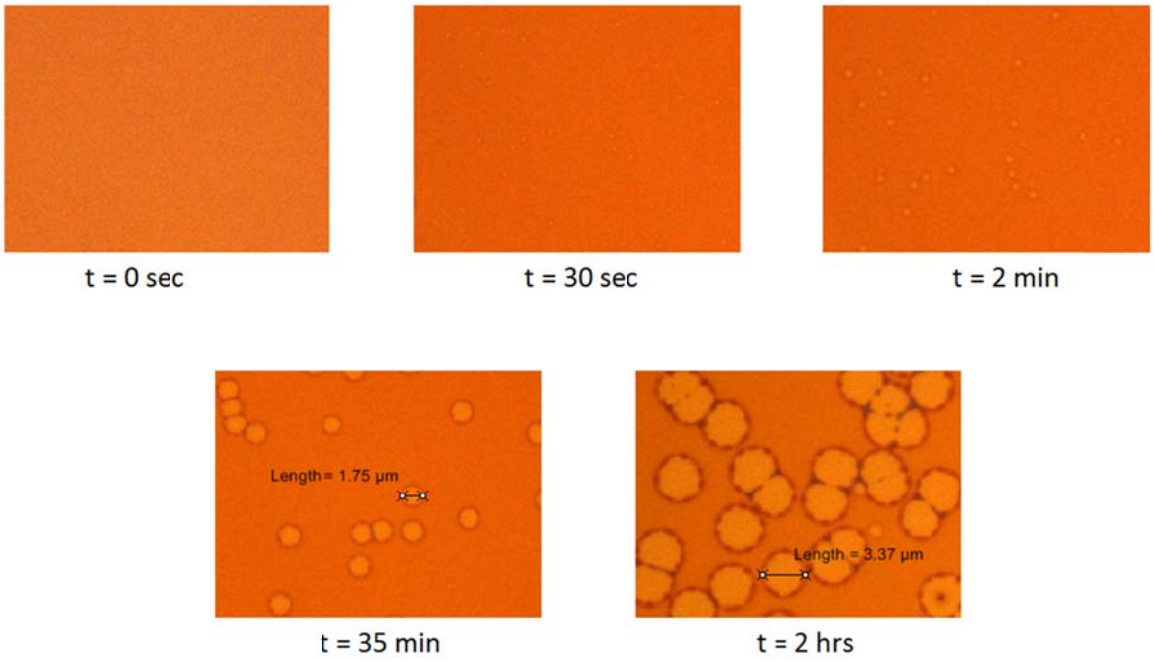

Figure 30. PS film spin-coated on top of a deprotected polymer film and then heated.

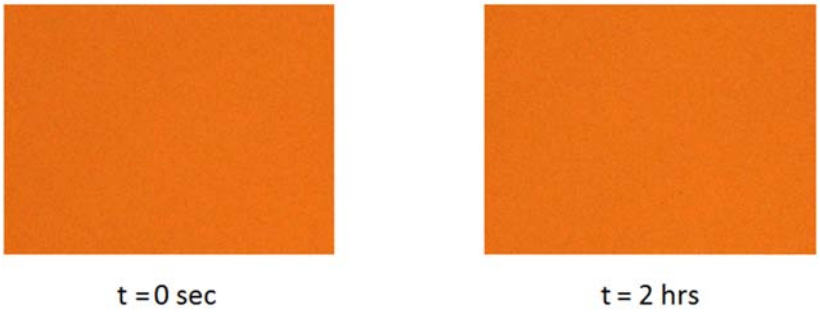

Figure 31. PS film spin-coated on top of a polymer film with active catalyst. The film was deprotected and dewetted at 110 °C.

When the underlying photoresist did not include active catalyst(Figure 29 and Figure 30), the PS film dewets at 110 °C. This outcome is independent of the deprotection level in the film. However, when the film contains active catalyst (Figure 31), no dewetting occurred. The origin of this behavior is unclear. Crosslinking of PS could inhibit dewetting, but PS is inert to the acid catalyst. This was verified with the following experiment. It was possible that the outgassing by-product could be cross-

linking the PS. Therefore, another experiment was done to check if cross-linking was actually occurring. A 35 nm PS (75kg/mol) with 14.5×10^{-2} nm^{-3} triflate was spin-coated on a silicon wafer. The film was baked at 110 °C for 10 minutes to remove excess solvent and the catalyst was activated by exposure to UV light. The film was baked at 110 °C for another 2 hours and immersed in toluene for 20 seconds. If PS crosslinks, then it becomes insoluble in toluene. The thickness summaries are shown in Table 11. Since most of the film was removed from the silicon wafer in both active and inactive catalyst cases, cross-linking was not occurring and cannot explain the lack of dewetting of PS during deprotection reaction. Therefore, the next step would be find another way to understand why the dewetting does not occur, as this method could offer a new way to stabilize and/or pattern thin films. Other methods will be devised to test for local heating, likely based on infrared imaging.

Table 11. Thickness measurement before and after immersion in toluene for 20 seconds.

	Thickness (before) nm	**Thickness (after toluene) nm**
Inactive catalyst	34.8	3.62
Active catalyst	37	4.6

BIBLIOGRAPHY

(1) Moore, G. E. Cramming More Components Onto Integrated Circuits. *Proc. IEEE* **1998**, *86* (1), 82–85.

(2) Zhang, G.; Wang, D. Colloidal Lithography—The Art of Nanochemical Patterning. *Chem. – Asian J.* **2009**, *4* (2), 236–245.

(3) Ito, H. Chemical Amplification Resists: History and Development within IBM (Reprinted from IBM Journal of Research and Development, Vol 41, 1997). *Ibm J. Res. Dev.* **2000**, *44* (1-2), 119–130.

(4) Shirai, M.; Tsunooka, M. Photoacid and Photobase Generators: Chemistry and Applications to Polymeric Materials. *Prog. Polym. Sci.* **1996**, *21* (1), 1–45.

(5) Prabhu, V. M.; Kang, S.; VanderHart, D. L.; Satija, S. K.; Lin, E. K.; Wu, W. Photoresist Latent and Developer Images as Probed by Neutron Reflectivity Methods. *Adv. Mater.* **2011**, *23* (3), 388–408.

(6) Meares, P. The Diffusion of Gases Through Polyvinyl Acetate1. *J. Am. Chem. Soc.* **1954**, *76* (13), 3415–3422.

(7) Vrentas, J. S.; Liu, H. T.; Lau, M. K. *Appl. Polm. Sci.* **1982**, 27,3987.

(8) Koros, W. J.; Hellums, M. W. Transport Properties. In *Encyclopedia of Polymer Science and Engineering*; 1989.

(9) Amergedon, Van G. J. *Rubber Chem. Technol.* **1951**, 24,109.

(10) Munk, P. *Introduction to Macromolecular Science*; Wiley: New York, 1989.

(11) Williams, M. L.; Landel, R. F.; Ferry, J. D. The Temperature Dependence of Relaxation Mechanisms in Amorphous Polymers and Other Glass Forming Liquids. *Am. Chem. Soc.* **1955**, *77*, 3701.

(12) Fryer, D. S.; Bollepali, S.; Pablo, J. J. de; Nealey, P. F. Study of Acid Diffusion in Resist near the Glass Transition Temperature. *J. Vac. Sci. Technol. B* **1999**, *17* (6), 3351–3355.

(13) Barrer, R. M. *Diffusion in and through Solids*; Cambridge University Press: Great Britain, 1951.

(14) Ganesh, K.; Nagarajan, R.; Duda, J. Rate of Gas-Transport in Glassy-Polymers - a Free-Volume Based Predictive Model. *Ind. Eng. Chem. Res.* **1992**, *31* (3), 746–755.

(15) Azuma, T.; Niiyama, H.; Sasaki, H.; Mori, I. The Role of the Residual Solvent for Chemical Amplification Resists. *J. Electrochem. Soc.* **1993**, *140* (11), 3158–3161.

(16) Schlegel, L.; Ueno, T.; Hayashi, N.; Iwayanagi, T. Determination of Acid Diffusion in Chemical Amplification Positive Deep-Uv Resists. *Jpn. J. Appl. Phys. Part 1-Regul. Pap. Short Notes Rev. Pap.* **1991**, *30* (11B), 3132–3137.

(17) Ishii, T.; Matsuda, T. Contrast Enhancement of Sal Resist by Reducing Residual Solvent at Prebake. *Jpn. J. Appl. Phys. Part 2-Lett.* **1991**, *30* (7A), L1215–L1217.

(18) Tam, N. N.; Ferguson, R. A.; Neureuther, A. R. Practical Cage□effect Model for Crosslinking in a Negative Chemically Amplified Resist and Its Use in Comparing E□beam and Optical Exposure. *J. Vac. Sci. Technol. B* **1992**, *10* (6), 2565–2569.

(19) Postnikov, S. V.; Stewart, M. D.; Tran, H. V.; Nierode, M. A.; Medeiros, D. R.; Cao, T.; Byers, J.; Webber, S. E.; Wilson, C. G. Study of Resolution Limits due to Intrinsic Bias in Chemically Amplified Photoresists. *J. Vac. Sci. Technol. B* **1999**, *17* (6), 3335–3338.

(20) Itani, T.; Yoshino, H.; Hashimoto, S.; Yamana, M.; Samoto, N.; Kasama, K. Relationship between Remaining Solvent and Acid Diffusion in Chemically

Amplified Deep Ultraviolet Resists. *Jpn. J. Appl. Phys.* **1996**, *35* (Part 1, No. 12B), 6501–6505.

(21) Goldfarb, D. L.; Angelopoulos, M.; Lin, E. K.; Jones, R. L.; Soles, C. L.; Lenhart, J. L.; Wu, W. Confinement Effects on the Spatial Extent of the Reaction Front in Ultrathin Chemically Amplified Photoresists. *J. Vac. Sci. Technol. B* **2001**, *19* (6), 2699–2704.

(22) Lin, E. K.; Soles CL; Goldfarb, D. L.; Trinque BC; Burns SD. Direct Measurement of the Reaction Front in Chemically Amplified Photoresists. *Science* **2002**, *297* (5580), 372–375.

(23) Stewart, M. D.; Becker, D. J.; Stachowiak, T. B.; Schmid, G. M.; Michaelson, T. B.; Tran, H. V.; Willson, C. G. Acid Mobility in Chemically Amplified Photoresists; 2002; Vol. 4690, pp 943–951.

(24) Wallraff, G.; Hutchinson, J.; Hinsberg, W.; Houle, F.; Seidel, P.; Johnson, R.; Oldham, W. Thermal and Acid-catalyzed Deprotection Kinetics in Candidate Deep Ultraviolet Resist Materials. *J. Vac. Sci. Technol. B* **1994**, *12* (6), 3857–3862.

(25) Nakamura, J.; Ban, H.; Tanaka, A. Influence of Acid Diffusion on the Lithographic Performance of Chemically Amplified Resists. *Jpn. J. Appl. Phys. Part 1-Regul. Pap. Brief Commun. Rev. Pap.* **1992**, *31* (12B), 4294–4300.

(26) Krasnoperova, A.; Khan, M.; Rhyner, S.; Taylor, J.; Zhu, Y.; Cerrina, F. Modeling and Simulations of a Positive Chemically Amplified Photoresist for X-Ray-Lithography. *J. Vac. Sci. Technol. B* **1994**, *12* (6), 3900–3904.

(27) Zuniga, M.; Neureuther, A. R. Reaction-diffusion Modeling and Simulations in Positive Deep Ultraviolet Resists. *J. Vac. Sci. Technol. B* **1995**, *13* (6), 2957–2962.

(28) Kang, S. H.; Prabhu, V. M.; Vogt, B. D.; Lin, E. K.; Wu, W.; Turnquest, K. Effect of Copolymer Composition on Acid-Catalyzed Deprotection Reaction Kinetics in Model Photoresists. *Polymer* **2006**, *47* (18), 6293–6302.

(29) Kang, S.; Lavery, K.; Choi, K.-W.; Prabhu, V. M.; Wu, W.-L.; Lin, E. K.; De Silva, A.; Felix, N.; Ober, C. A Comparison of the Reaction-Diffusion Kinetics between Model-EUV Polymer and Molecular-Glass Photoresists; 2008; Vol. 6923, pp 692317–692317 – 12.

(30) Kang, S.; Wu, W.; Choi, K.-W.; De Silva, A.; Ober, C. K.; Prabhu, V. M. Characterization of the Photoacid Diffusion Length and Reaction Kinetics in EUV Photoresists with IR Spectroscopy. *Macromolecules* **2010**, *43* (9), 4275–4286.

(31) Perera, G. M.; Pandey, Y. N.; Patil, A. A.; Stein, G. E.; Doxastakis, M. Reaction Kinetics in Acid-Catalyzed Deprotection of Polymer Films. *J. Phys. Chem. C* **2012**, *116* (46), 24706–24716.

(32) Reichmanis, E.; Houlihan, F. M.; Nalamasu, O.; Neenan, T. X. Chemical Amplification Mechanisms for Microlithography. *Chem. Mater.* **1991**, *3* (3), 394–407.

(33) *Nicolet FT-IR User Guide*; Thermo Electron Corporation: Madison, WI, 2004.

(34) Wade, L. G. Organic Chemistry; Prentice Hall: New Jersey, 1999; p 500.

(35) Tan, T. L.; Kudryashov, V. A.; Tan, B. L. FT-IR Study of a Chemically Amplified Resist for X-Ray Lithography. *Appl. Spectrosc.* **2003**, *57* (7), 842–849.

(36) Houle, F. A.; Hinsberg, W. D.; Morrison, M.; Sanchez, M. I.; Wallraff, G.; Larson, C.; Hoffnagle, J. Determination of Coupled Acid Catalysis-Diffusion Processes in a

Positive-Tone Chemically Amplified Photoresist. *J. Vac. Sci. Technol. B* **2000**, *18* (4), 1874–1885.